IRAQI JOURNAL OF APPLIED PHYSICS

The *Iraqi Journal of Applied Physics (IJAP)* is a peer reviewed journal of high quality devoted to the publication of original research papers from applied physics and their broad range of applications. IJAP publishes quality original research papers, comprehensive review articles, survey articles, book reviews, dissertation abstracts in physics and its applications in the broadest sense. It is intended that the journal may act as an interdisciplinary forum for Physics and its applications. Innovative applications and material that brings together diverse areas of Physics are particularly welcome. Review articles in selected areas are published from time to time. It aims to disseminate knowledge; provide a learned reference in the field; and establish channels of communication between academic and research experts, policy makers and executives in industry, commerce and investment institutions. IJAP is a quarterly specialized periodical dedicated to publishing original papers, letters and reviews in: Applied & Nonlinear Optics, Applied Mechanics & Thermodynamics, Digital & Optical Communications, Electronic Materials & Devices, Laser Physics & Applications, Plasma Physics & Applications, Quantum Physics & Spectroscopy, Semiconductors & Optoelectronics, and Solid State Physics & Applications

SPONSORED AND PUBLISHED BY
THE IRAQI SOCIETY FOR ALTERNATIVE AND RENEWABLE ENERGY SOURCES & TECHNIQUES (I.S.A.R.E.S.T.)

IRAQI JOURNAL OF APPLIED PHYSICS
" INSTRUCTIONS TO AUTHORS "

CONTRIBUTIONS

Contributions to be published in this journal should be original research works, i.e., those not already published or submitted for publication elsewhere, individual papers or letters to editor.

SUBMISSION OF MANUSCRIPTS

Manuscripts should be submitted to the editor at the mailing address:

Iraqi Journal of Applied Physics
Editorial Board
P. O. Box 55259, Baghdad 12001, IRAQ, submission@ijap.org , editor@ijap.org

MANUSCRIPTS

Two hard copies with soft copy on a compact disc (CD) should be submitted to Editor in the following configuration:

- Double-spaced one-side A4 size with 2.5 cm margins of all sides
- Times New Roman font (16pt bold for title, 14pt bold for names, 12pt bold for headings, 12pt regular for text)
- Letters should not exceed 10 pages, papers should not exceed 20 pages and reviews are up to author.
- Manuscripts presented in English only are accepted.
- English abstract not exceed 150 words
- 4 keywords (at least) should be maintained on (PACS preferred)
- Author(s) should express all quantities in SI units
- Equations should be written in equation form (*italic* and symbolic)
- Figures and Tables should be separated from text
- Figures and diagrams can be submitted in colors for assessment and they will be returned to authors after provide printable copies
- Charts should be indicated by the software used for
- Only original or high-resolution scanner photos are accepted
- For electronic submission, articles should be formatted with MS-Word software.

AUTHOR NAMES AND AFFILIATIONS

It is IJAP policy that all those who have participated significantly in the technical aspects of a paper be recognized as co-authors or cited in the acknowledgments. In the case of a paper with more than one author, correspondence concerning the paper will be sent to the first author unless staff is advised otherwise.

Author name should consist of first name, middle initial, last name. The author affiliation should consist of the following, as applicable, in the order noted:

- Company or college (with department name or company division)
- Postal address
- City, state, zip code
- Country name
- Telephone, and e-mail

REFERENCES

The references should be brought at the end of the article, and numbered in the order of their appearance in the paper. The reference list should be cited in accordance with the following examples:

[1] X. Ning and M.R. Lovell, "On the Sliding Friction Characteristics of Unidirectional Continuous FRP Composites", *ASME J. Tribol.*, 124(1) (2002) 5-13.
[2] M. Barnes, "Stresses in Solenoids", *J. Appl. Phys.*, 48(5) (2001) 2000–2008.
[3] J. Jones, "Contact Mechanics", Cambridge University Press (Cambridge, UK) (2000), Ch.6, p.56.
[4] Y. Lee, S.A. Korpela and R. Horne, "Structure of Multi-Cellular Natural Convection in a Tall Vertical Annulus", Proc. 7th International Heat Transfer Conference, U. Grigul et al., eds., Hemisphere (Washington DC), 2 (1982) 221–226.
[5] M. Hashish, "Waterjet Technology Development", High Pressure Technology, PVP-Vol. 406 (2000), 135-140.
[6] D.W. Watson, "Thermodynamic Analysis", ASME Paper No. 97-GT-288 (1997).
[7] C.Y. Tung, "Evaporative Heat Transfer in the Contact Line of a Mixture", Ph.D. thesis, Rensselaer Polytechnic Institute, Troy, NY (1982).

PROOFS

Authors will receive proofs of papers and are requested to return one corrected hard copy with a WORD copy on a compact disc (CD). New materials inserted in the original text without Editor permission may cause rejection of paper.

COPYRIGHT FORM

Author(s) will be asked to transfer copyrights of the article to the Journal soon after acceptance of it. This will ensure the widest possible dissemination of information.

OFFPRINTS

Authors will receive offprints free of charge and any additional offprints can be ordered.

SUBSCRIPTION AND ORDERS

Annual fees (4 issues per year) of subscription are:

- 50 US$ for individuals inside Iraq.
- 100 US$ for establishments inside Iraq.
- 100 US$ for individuals abroad.
- 200 US$ for establishments abroad.

Fees are reduced by 25% for I.S.A.R.E.S.T. members. Orders of issues can be submitted by contacting the editor-in-chief or editorial office at **subscription@ijap.org** to maintain the address of issue delivery and payment way.

Invited Paper

Technology and Future of III-V Multi-Junction Solar Cells

Steven Lansel

School of Electrical and Computer Engineering, Georgia Institute of Technology, Atlanta, GA, U.S.A

Multi-junction solar cells created from III-V semiconductor materials exhibit high efficiencies matched by no other existing photovoltaic technology. Multi-junction solar cells are composed of 3 layers of material that have different bandgaps. The top layer has the largest bandgap while the bottom layer has the smallest bandgap. This design allows less energetic photons to pass through the upper layer(s) and be absorbed by a lower layer, which increases the overall efficiency of the solar cell. One important design consideration is that the photocurrent generated in each layer must be the same since the layers are in series. In addition, the bandgaps of each layer should differ by approximately equal energies so that the spectrum of incident radiation is most effectively absorbed. Although multi-junction solar cells are very efficient, they are also very expensive. Due to their high cost, multi-junction solar cells are primarily used in systems in outer space and as collector cells where a large amount of sunlight is reflected onto the cell. The use of multi-junction solar cells made of III-V semiconductor materials appears to be restricted to limited applications while single crystalline silicon semiconductors have a wider application due to the lesser cost. This paper will focus on the present and future design, practical and theoretical efficiency, and applications of III-V multi-junction solar cells.

Keywords: Solar cells, Multijunction devices, III-V compounds, Quantum efficiency
Received: 05 June 2010, **Accepted**: 12 June 2010

1. Introduction

One of the largest challenges mankind will face in the twenty-first century and beyond is how to supply our increasing need for energy. With the rapid consumption rate of fossil fuels, we need to consider renewable energy sources such as photovoltaics. Photovoltaics are a promising technology that directly takes advantage of our planet's ultimate source of power, the sun. When exposed to light, solar cells are capable of producing electricity without any harmful effect to the environment or device, which means they can generate power for many years while requiring only minimal maintenance and operational costs. Currently the wide-spread use of photovoltaics over other energy sources is limited by the relatively high cost and low efficiency of solar cells.

Multijunction solar cells are a new technology that offers extremely high efficiencies compared to traditional solar cells made of a single layer of semiconductor material. Depending on the particular technology, multijunction solar cells are capable of generating approximately twice as much power under the same conditions as traditional solar cells made of silicon. Unfortunately, multijunction solar cells are very expensive and are currently only used in high performance applications such as satellites due to their cost.

This paper will investigate the design of multijunction solar cells. First, fundamentals of solar cell operation and performance will be presented. The basic advantage and operation of multijunction solar cells will be discussed. Then, the paper will discuss important design issues. Current solar cell design and performance will be presented. Then, future design improvements will be offered. Finally, the paper will conclude with an argument that the design of multijunction solar cells will improve in the near future and the technology can become a viable widespread power source.

2. Fundamental Solar Cell Concepts

Solar cells are semiconductor devices that are designed to generate electric power when exposed to electromagnetic radiation. The spectrum of light given off by the sun is shown in Figure 1. The distribution of light in outer space resembles the theoretical radiation provided by a black body. As the light passes through the atmosphere, some of the light is absorbed or reflected by gasses such as water vapor and the ozone. For this reason, the typical distribution of light on the surface of the earth shown in Figure 1 is different than the distribution of light in space. Engineers must consider the spectrum of incident light when designing solar cells.

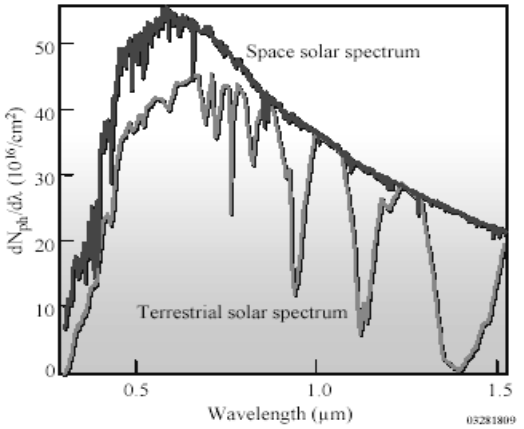

Fig. (1) Spectrum of solar radiation in space and on earth [2]

Solar cells consist of one or more p-n junctions. Light enters the semiconductor material through the n region and generates an electron-hole pair (EHP) in the material due to the photoelectric effect. The n region is designed to be thin while the depletion region is thick. If the EHP is generated in the depletion region, the built-in electric field drifts the electron and hole apart. The result is a current through the device called the photocurrent. If the EHP is generated in the n or p regions, the electron and hole drift in random directions and may or may not become part of the photocurrent [1].

The following terms deal with the performance of a solar cell:

- **Short-circuit current, J_{sc}:** The current of a solar cell when the top and bottom (negative and positive leads) are connected with a short circuit. This is the horizontal intercept on the I-V curve shown in Figure 2.
- **Open-circuit voltage, V_{OC}:** The voltage between the top and bottom of a solar cell. This is the vertical intercept on the I-V curve shown in Figure 2.
- **Power point:** The point on the I-V curve of a solar cell at (J_{PP}, V_{PP}) that generates the maximum amount of power for the device. This is the point that encloses the most amount of area in the first quadrant when vertical and horizontal lines are drawn from the point. This represents power since the area is equivalent to the current times voltage of the cell. The power point is shown in Figure 2.
- **Fill factor, FF:** A percentage given by Equation 1 that describes how close the I-V curve of a solar cell resembles a perfect rectangle, which represents the ideal solar cell.

$$\text{Fill Factor} = \frac{V_{PP} * J_{PP}}{V_{OC} * J_{SC}} \quad (1)$$

- **Quantum efficiency:** The number of EHPs that are created and collected divided by the number of incident photons [1]. This is a percentage since each photon can produce at most one EHP.
- **Overall efficiency:** The percent of incident electromagnetic radiation that is converted to electrical power. Often the overall efficiency for a given solar cell depends on many factors including the temperature and amount of incident radiation.

2.1 Multijunction Solar Cells

With a traditional single layer solar cell, much of the energy of incident light is not converted into electricity. If an incident photon has less energy than the bandgap of the semiconductor material, the photon cannot be absorbed since there is not enough energy to excite an electron from the conduction band to the valence band. Therefore, none of the light with less energy than the bandgap is used in the solar cell. If an incident photon has more energy than the bandgap, the excess energy will be converted into heat since the electron can only absorb the exact amount of energy required to move to the valence band.

Multijunction solar cells can make better use of the solar spectrum by having multiple semiconductor layers with different bandgaps. Each layer is made of a different material, which usually is a III-V semiconductor, and absorbs a different portion of the spectrum. The top layer has the largest bandgap so that only the most energetic photons are absorbed in this layer. Less energetic photons must pass through the top layer since they are not energetic enough to generate EHPs in the material. Each layer going from the top to the bottom has a smaller bandgap than the previous. Therefore, each layer absorbs the photons that have energies greater than the bandgap of that layer and less than the bandgap of the higher layer. The most common form of multi-junction solar cell consists of three layers, which is called a triple-junction solar cell.

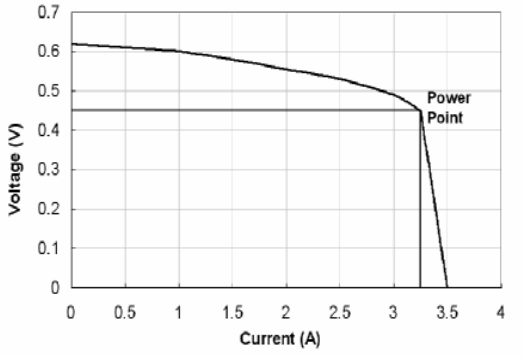

Fig. (2) Current versus voltage curve (I-V curve) for a typical solar cell [3]

2.2 Design Considerations

2.2.1 Bandgaps

Since the bandgaps of the materials used in a multijunction solar cell determine which layer a photon is absorbed in, the bandgaps determine how much energy can be obtained from each photon. Ideally the difference between adjacent layers of the solar cell is approximately constant so that each layer can absorb an equal amount of the spectrum of incident light shown in Figure 1. Since the amount of excess energy from light converted to heat is equal to the difference between the photon energy and the bandgap of the absorbing material, the difference between bandgaps should be made as small as possible. Also the solar cell should take advantage of as much of the spectrum as possible so the top layer should have a high bandgap and the bottom layer should have a small bandgap that can absorb as much of the spectrum as possible. Clearly there is a design tradeoff for a given number of layers of a multijunction solar cell between having the bandgaps differ by a small amount and have the bandgaps cover a large range of the spectrum. Triple-junction solar cells currently in production are made of GaInP, GaAs, and Ge, which have bandgaps of 1.8 eV, 1.4 eV, and 0.7 eV, respectively [2].

2.2.2 Lattice Constant

In monolithic multijunction solar cells, the different semiconductor layers are grown directly on top of the other layers using the same substrate. As a result of this method, the lattice constant, which describes the spacing of the molecules of a crystal structure, must be the same for all of the layers. Research at the Natoinal Renewable Energy Laboratory (NREL) showed that a lattice mismatch as small as 0.01% significantly decreases the current produced by the solar cell [4]. The restriction of each semiconductor material having the same lattice constant significantly decreases the number of materials that may be used. Figure 3 shows the lattice constant and bandgap of common semiconductor materials.

Lines between different materials represent semiconductors that are created by combining different amounts of the two materials. The vertical line passing through Ge represents the materials that are used to create the current triple-junction cells made of GaInP, GaAs, and Ge.

2.2.3 Current Matching

Since the current flows through a solar cell from the top to the bottom, the layers of a multijunction solar cell are in series. Therefore, the current passing through each layer must be the same and the current produced by the solar cell is limited by the layer that produces the least amount of current. For maximum efficiency, the cell must be designed so that each layer produces the exact same current. The current is proportional to the number of photons absorbed in each layer. The two most important factors in determining the thickness of each layer is the number of photons in the spectrum that the layer should absorb and the absorption constant of the material. The light intensity decreases exponentially with penetration depth into a material where the exponential constant is called the absorption constant [1:221]. A layer with a low absorption constant must be made thicker since on average a photon must pass through more of the material before it is absorbed. Properly designing the thickness of each semiconductor material based on these factors will match the current produced by each layer.

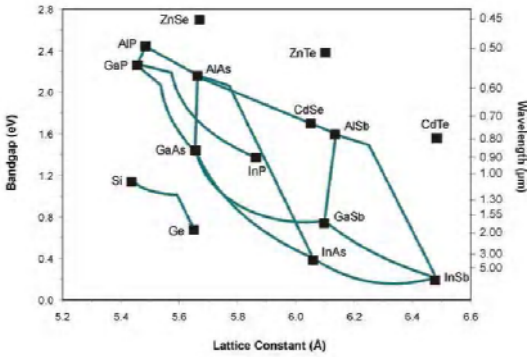

Fig. (3) Lattice constant and bandgap of common semiconductor materials [5]

2.2.4 Layer Thickness Calculation

After materials are selected with desired bandgaps and lattice constants, the thickness of each layer must be determined so that each layer will generate the same photocurrent. In this section, I will go through a rough calculation to determine the proper thickness of each layer of a GaInP/GaAs/Ge triple-junction solar cell. The calculation would be much more precise and useful if experimental data was used in the calculation.

In determining the thickness of each layer, the most important difference between semiconductor materials is the material's absorption constant and the number of incident photons with a given energy. The absorption constant as a function of photon wavelength for various semiconductors is provided in Figure 4. The absorption constant as a function of photon energy for $(Al_xGa_{1-x})_{0.52}In_{0.48}P$ is provided in Figure 5. When x=0, the graph shows the alpha for GaInP. The photocurrent generated by each layer is approximately proportional to the number of photons absorbed in the layer. I am assuming that the quantum efficiency of the

 ISSN 1813-2065

different materials is made to be approximately equal, which will be justified later. Therefore, we want to determine the thickness of each layer so that the number of photons absorbed in each layer is equal, which is a function of alpha for each material.

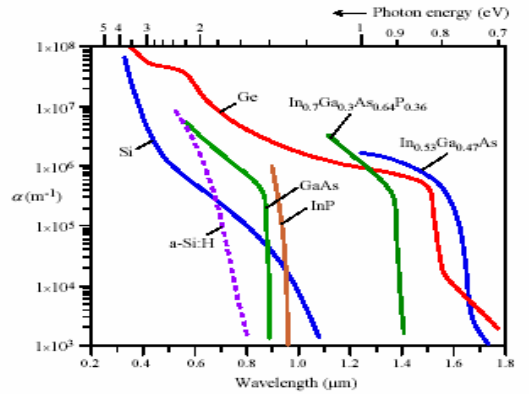

Fig. (4) Absorption coefficient vs wavelength for various semiconductor materials [1]

In the calculation, I assume that the incident solar radiation is given by Planck's Law for blackbody radiation, which is given in Equation 2 where T=6000 K for the sun.

$$I(\nu) = \frac{2h\nu^3}{c^2 * \exp\left(\frac{h\nu}{kT} - 1\right)} \qquad (2)$$

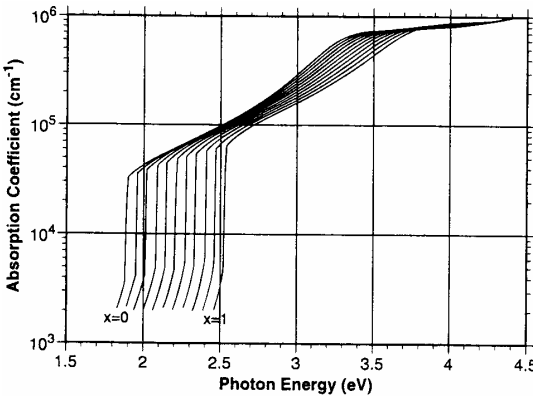

Fig. (5) Absorption coefficient vs photon energy for (AlxGa1-x)0.52In0.48P [9]

The blackbody assumption is fairly accurate for outer space but is inaccurate on the earth's surface due to absorption in the atmosphere as shown in Figure 1. The assumption could be used with some accuracy for design of solar cells for use in space but would prove poor for terrestrial solar cells.

The thickness calculation performed in Maple is provided in Appendix A. After deriving expressions for the photocurrent generated in each layer, the currents were matched. A reasonable cutoff for the Ge layer was then calculated to be approximately 40 μm. In practice, terrestrial solar cells are designed so that the Ge layer is fixed at 150 μm and the thickness of the other two layers is designed to match the current [8].

2.2.5 Triple-Junction Solar Cell

The most powerful multi-junction solar cells in commercial production today are triple-junction cells made of GaInP, GaAs, and Ge. Only two companies, Emcore and Spectrolab, are currently producing these highly efficient cells and are licensing technology from the National Renewable Energy Laboratory (NREL). The first cell design created by Emcore was the 3J or TJ (triple-junction) cell. Later improvements resulted in the more efficient ATJ (advanced triple-junction) cell [6]. The I-V curve and performance parameters for typical 3J and ATJ solar cells are shown in Figure 6. Typical efficiencies for these types of cells are 26% and 27.5%, which is far greater than the typical efficiency of 16% for terrestrial silicon cells [6].

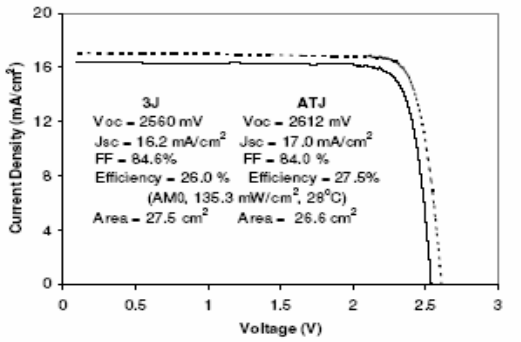

Fig. (6) Typical I-V curves for 3J and ATJ solar cells [6]

Viewing the quantum efficiency of each layer of the ATJ cells, which is shown in Figure 7, gives insight into the performance of each layer. Overall the quantum efficiency is high for the solar cell since it is near 90% for most wavelengths. The transitions between which layer absorbs a light of a given wavelength is due to the fact that the wavelength dictates the photon's energy and which layer can absorb it.

There is a sharp transition between the GaAs and Ge layers; however, the transition between the InGaP and GaAs layers is gradual and can be improved. The energy of photons that have wavelengths below approximately 650 nm and pass through the InGaP into the GaAs layer is not being efficiently captured. Ideally the InGaP layer would absorb all photons that are above the wavelength corresponding to the bandgap of GaAs. It can be seen that the germanium layer absorbs a larger portion of the spectrum then the other two layers, which is a result of the large difference between the bandgaps of GaAs and Ge.

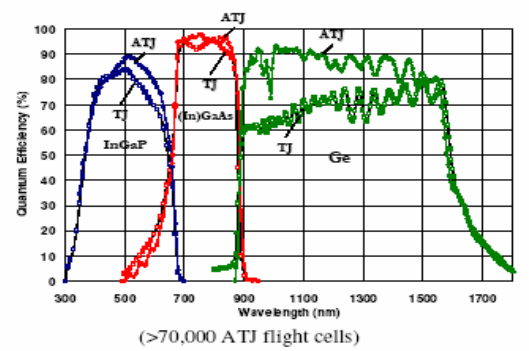

Fig. (7) Quantum efficiency for each layer of TJ and ATJ cells [7]

2.3 Future Design Improvements

The current use of GaInP, GaAs, and Ge for the layers of a multi-junction solar cell can be improved. The germanium layer absorbs too much of the spectrum, since the difference between the bandgap of the top two layers is 0.4 eV while the difference between the bottom two layers is 0.7 eV. Using a new semiconductor layer that has a bandgap of 1.25 eV will make the cell more efficient since the bandgaps will differ by a constant 0.55 eV. Another possible design improvement keeps the three GaInP, GaAs, and Ge layers but adds another layer of a material with a bandgap of 1.0 eV. This new four-junction solar cell will have a difference of 0.3 eV or 0.4 eV between each adjacent layer.

The distribution of the spectrum into which layer absorbs each wavelength for these proposed solar cell designs is provided in Figure 8. The theoretical and practical efficiencies for these new technologies under standard terrestrial illumination are shown to exceed 40% and 32%, respectively, with higher efficiencies possible for increased illumination [8]. In addition, to the bandgap requirements of a new semiconductor material, it also must match the lattice constant of germanium in order to be feasible.

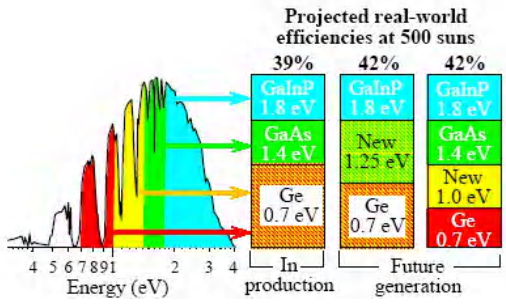

Fig. (8) Efficiencies and spectrum division based on layer for current and future multi-junction solar cells [2]

Fig. (9) Example of a collector cell apparatus [2]

3. Discussion

Multijunction cells made of III-V semiconductor materials offer much higher efficiencies then single layer cells and especially traditional silicon solar cells. Right now these cells are primarily used in space applications since they are so expensive. Currently solar cells under typical illumination levels found on the surface of the earth produce efficiencies in the high 20's. With improvements to multijunction solar cell design and better semiconductor materials, these efficiencies can be increased to the high 30's in the near future. Although the production and materials cost will decrease with further advances and large-scale production, multijunction solar cells will still be far more expensive than regular silicon solar cells. This is due to the fact that the multijunction cells are much more complex and use materials that are rarer than silicon. As a result, multijunction cells must be used differently than other solar cells. Multijunction cells can be used as viable power sources by building an apparatus that directs a large amount of incident light onto a small area of solar cells, which is referred to as a collector cell. A picture of a collector cell apparatus is provided in Figure 9. In this application, the solar cells must be extremely efficient and the cost is not a consideration since only a small number of cells are used to generate a large amount of electricity.

4. Conclusions

Multijunction solar cells work by layering semiconductor materials that have different bandgaps. Light enters through the layer that has the largest bandgap. Depending on the energy of the photon, it penetrates the solar cell until it reaches a layer that has a smaller bandgap than the photon's energy. Using this concept, multijunction solar cells are more efficient than single layer solar cells. This is because less of the energy of a photon exceeds the bandgap of the absorbing semiconductor, which is energy lost to heat.

ISSN 1813-2065

There are a number of factors involved in the design of multijunction solar cells. The materials used in the cell must all have the same lattice constant. In addition, the bandgaps of the semiconductors should divide the spectrum of incident light into approximately equal regions and also span most of the spectrum so that all incident light is absorbed efficiently. The thickness of each layer in the solar cell must be adjusted so that each layer produces the same amount of current since the layers are in series.

The most efficient solar cells in production today are triple-junction cells made of GaInP, GaAs, and Ge that achieve typical efficiencies of 27.5%. The current design can be improved by finding a semiconductor material with a bandgap of approximately 1.0 eV or 1.25 eV that has the same lattice constant as germanium. Although the price of multijunction solar cells will decrease in the future, they will remain expensive but can still be used in collector cells for effective power production.

References

[1] S.O. Kasap, **"Optoelectronics and Photonics: Principles and Practices"**, Prentice Hall (NY) (2001).

[2] B. Burnett "The Basic Physics and Design of III-V Multijunction Solar Cells", 2002 from: http://www.nrel.gov/ncpv/pdfs/11_20_dga_basics_9-13.pdf

[3] D.R. Carroll, The Winning Solar Car, Warrendale: SAE International, 2003.

[4] R.R. King et al., "Advances in High-Efficiency Multijunction Terrestrial Concentrator Cells and Receivers," in *Proc.* of NCPV and Solar Program Review Meeting 2003, 211.

[5] J.M. Román, "State-of-the-art of III-V Solar Cell Fabrication Technologies, Device Designs and Applications", *Adv. Photovolt. Cell Design*, 2004.

[6] M.A. Stan et al., "27.5% Efficiency InGaP/InGaAs/Ge Advanced Triple Junction (ATJ) Space Solar Cells for High Volume Manufacturing" in *Proc.* of the 29th IEEE Photovoltaic Specialists Conf., 2002, 816-819.

[7] M.A. Stan et al., "Design and Production of Extremely Radiation-Hard 26% InGaP/GaAs/Ge Triple-Junction Solar Cells" in *Proc*. of the 28th IEEE Photovoltaic Specialists Conf., 2000, 1374-1377.

[8] S.R. Kurtz, D. Myers and J. M. Olson, "Projected Performance of Three- and Four-Junction Devices Using GaAs and GaInP," in *Proc*. of the 26th IEEE Photovoltaic Specialists Conf., 1997, 875-878.

[9] Y.N. Mohapatra, Epitaxy, (2005) from: http://home.iitk.ac.in/~ynm/People/YNM/Epitaxy.ppt.

This article was reviewed at School of Engineering, College of Engineering and Computing Sciences, The Australian National University, Australia, and School of Applied Sciences, University of Technology, Baghdad, Iraq

---

Ahmed E. Bekheet
Ali H. Ashor
Hani E. Atyia
Munir A. Afifi

Department of Physics, Faculty of Education, Ain Shams University, Roxy, Cairo, Egypt

DC Conductivity and Optical Properties of $InSbTe_3$ Amorphous Thin Films

Measurements of dc electrical conductivity and optical properties have been made on $InSbTe_3$ thin films prepared by thermal evaporation having different thickness (25-150) nm range. The structure of $InSbTe_3$ in its powder and thin film forms were investigated by X-ray diffraction (XRD). The electrical conductivity was measured in the temperature (303-392) K range. The obtained values of dc electrical conduction activation energy ΔE_σ were found to be nearly independent on the film thickness and have the mean value of 0.173 eV in the range considered. The refractive index n and the absorption index k were determined in the spectral range 400-2500 nm. It is observed that n decreases with increasing film thickness at any wave length, while k is practically independent on film thickness in the range 25-150 nm. For films with thicknesses in the range 170-304 nm, the spectral distribution of transmittance T and reflectance R showed that T+R<1 in the whole spectrum which due to light scattering by surface roughness whose existence is confirmed by electron microscopy. Analysis of k indicated that the absorption mechanism refers to the existence of indirect transitions with an optical energy gap of 0.52 eV.

Keywords: *DC conductivity, $InSbTe_3$, Amorphous, Thin film*
Received: 12 July 2010, **Revised**: 25 August 2010, **Accepted**: 01 September 2010

components were mixed inside a sealed evacuated silica tube (10^{-5} Pa) and melted using a constructed oscillatory furnace, which ensure the homogeneity of the composition. The furnace temperature was raised to 1003 K at a rate of $50Kh^{-1}$ [18] and kept constant for 48 hours. Then, the temperature of the furnace was decreased at a rate of 3 K min^{-1} to room temperature.

$InSbTe_3$ thin films of different thickness were prepared by thermal evaporation on dry-clean glass substrates under vacuum of 10^{-5} Pa using a coating unit (Edward 306 A). The film thickness was measured by Tolansky's interferometric method.

The structure of the investigated composition in powder and thin film forms was investigated by X-ray diffraction analysis by using a Philips X-ray diffractometer with Cu target and Ni filter operated at 36 kV and 20 mA to give X-rays with wavelength 1.542 A^o. The chemical composition was checked by energy dispersive X-ray analysis (EDX) using a scanning electron microscope (Joel 5400).

Dc conductivity was measured for thin films of different thicknesses, sandwiched between two Al electrodes. Their resistance R was measured using a digital electrometer (Keithley type E616A). The conductivity was calculated by the relation

$$\sigma_{dc} = \left(\frac{d}{A}\right)\frac{1}{R} \qquad (1)$$

1. Introduction

In_2Te_3 is a semiconductor material with a defect crystal structure which is of the sphalerite type and contains 5x 10^{-3} /cc empty neutral sites in the cation sublattice [1]. It has two phases (α and β) [2,3]. Many physical properties of In_2Te_3 were investigated earlier by several authors [1,4-7]. In_2Te_3 and its solid solutions have valuable photoelectrical properties, low sensitivity to impurities and low thermal conductivity. Sb_2Te_3 has narrow energy gap corresponding to weak polarity of bonds between Sb and Te. It is a low-resistively chalcogenide, whose solid solutions have good thermoelectric properties in the range (200-600K). Several authors investigated its electrical and optical properties [8-10].

The In_2Te_3–Sb_2Te_3 system ($Sb_{2-x}In_xTe_3$ solid solution) belongs to the family of layered compounds having the structure of space group D^5_{34}. Physical properties of single crystals of $Sb_{2-x}In_xTe_3$ compounds were described in a number of papers [11-15]. However, little attention was devoted to study physical properties for $InSbTe_3$ thin films [16-17].

This paper aimed to investigate the structure, electrical and optical properties of $InSbTe_3$ amorphous thin films with different thicknesses.

2. Experimental Procedure

$InSbTe_3$ compound was prepared in a bulk form by direct fusion of the 99.999 purity constituent elements In, Sb and Te. The

 ISSN 1813-2065 Printed in IRAQ

compounds and pure constituent elements, no line matching is observed.

The absence of the lines of binary compounds and pure constituent elements in the measured pattern shown in Fig. (1a) indicates the formation of $InSbTe_3$ ternary composition. Fig. (1b) shows the XRD patterns of $InSbTe_3$ thin films having different thicknesses in the (25-304) nm range. It is observed that all thin films in this range have an amorphous structure.

3.2 DC electrical conductivity

The room temperature dc electrical conductivity σ_{dc} for the as-deposited $InSbTe_3$ thin films of (50-150) nm thickness range was measured. The results are shown in Fig. (2). It is clear from this figure that σ_{dc} increases with increasing film thickness. This behaviour can be attributed to lattice defects, such as vacancies, interstitials and dislocations which might be distributed through the first stages of the film growth. These defects add extra percentages of resistivity. As the film thickness increases, these defects diffuse and the corresponding resistivity decreases, hence the conductivity increases with film thickness. The obtained room temperature dc electrical conductivity of the investigated films of the order of $10^{-6}\ \Omega^{-1}\ m^{-1}$ is higher than that for In_2Te_3 thin films with the same thickness ($\sim 10^{-7}\Omega^{-1}m^{-1}$) [6]. This is because the increase of Sb atoms increases the free carrier concentration [14,19] and hence increases the conductivity.

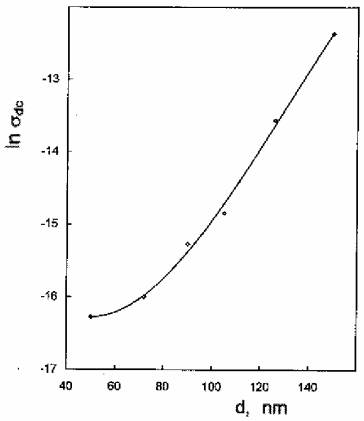

Fig. (2) Thickness dependence of room temperature dc conductivity σ_{dc} for $InSbTe_3$

The temperature dependence of electrical conductivity (σ_{dc}) was studied in the temperature range (303-393K) for the as-deposited films of the thickness (50-150) nm range. The obtained results illustrated in Fig.3, from which it is shown that the conductivity increases with increasing temperature. This behaviour indicating the presence of semiconducting properties of the $InSbTe_3$ thin films as that reported for other compounds [20] and may be due to the kinetic of the film growth and where d and A are the thickness and the cross-sectional area of the film, respectively

The optical properties of the as deposited thin films of different thicknesses were investigated. The transmission, T, and reflectance, R, of each film were measured at room temperature using a dual beam spectrophotometer (JASCO Corp.V-750, Rev.1.00.) equipped with unpolarized light at normal incidence in the spectral range from 500nm to 2500nm. Optical microscope photographs were made using optical microscope (Kyowo Tokyo No.873234 with magnification 1200) to clarify the nature of the film' surface.

3. Results and Discussion

3.1 Structural identification

EDX analysis indicated that the composition of the prepared material as powder and thin film forms are $In_{19.7}Sb_{17.3}Te_{63}$ and $In_{23.1}Sb_{18.81}Te_{58.09}$ respectively. This is close to $InSbTe_3$, with an experimental error of ±2%.

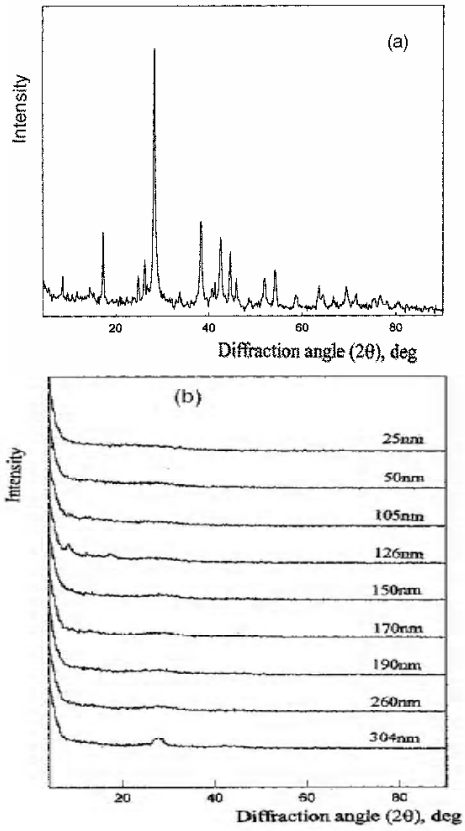

Fig. (1) (a) X-ray diffraction patterns of $InSbTe_3$ in powder form and (b) X-ray diffraction patterns of $InSbTe_3$ for thin films of different thicknesses

X-ray diffraction patterns for $InSbTe_3$ as powder form is given in Fig. (1a). This figure illustrate that the powder form has polycrystalline structures. In addition, by comparing the measured XRD pattern with the XRD patterns of In_2Te_3 and Sb_2Te_3 binary

absorption (small deviations from stoichiometry and contamination), or scattering of light by surface and volume imperfections [25] (surface roughness, rough internal boundaries and density fluctuations, etc [25]).

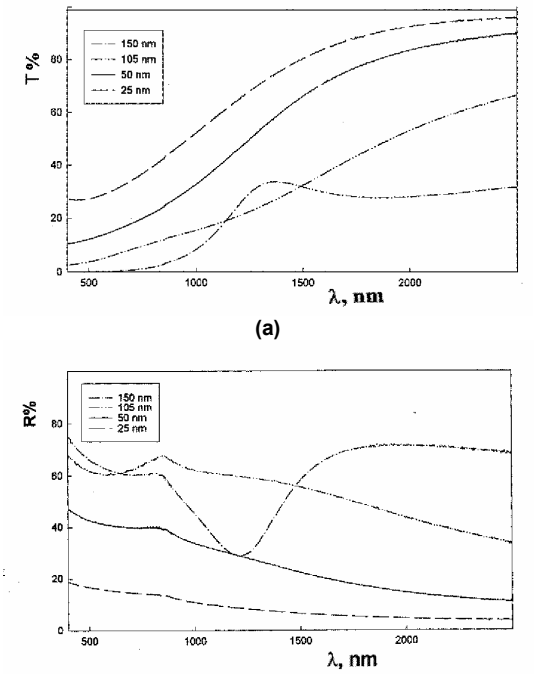

Fig. (4) Spectral distribution of (a) transmittance and (b) reflectance for $InSbTe_3$ thin films of different thicknesses in the (25-150) nm range

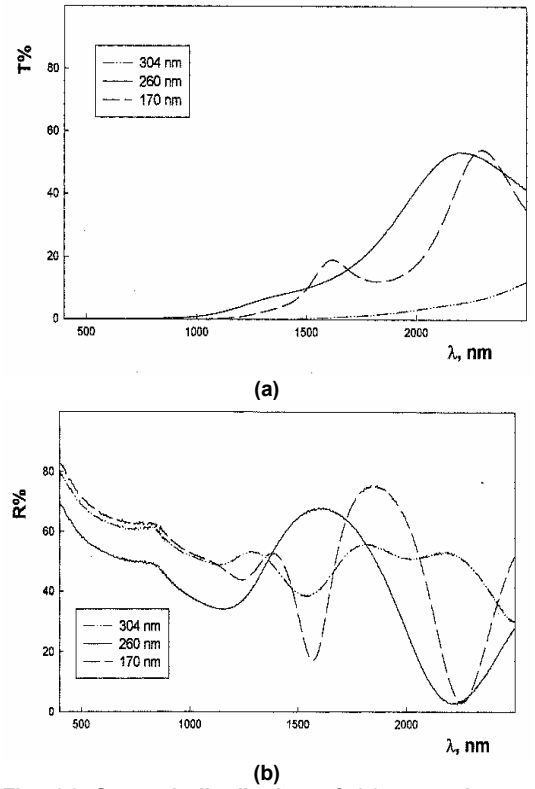

Fig. (5) Spectral distribution of (a) transmittance and (b) reflectance for $InSbTe_3$ thin films of different thicknesses in the (170-304) nm range

diminishing the density of structural defects [21]. The mean value of the activation energy of (0.173 eV) is calculated from the slopes obtained from the linear fit of measured data shown in Fig. (3) that also shows a set of nearly parallel straight lines, using the relation.

$$\sigma = \sigma_o \exp(-\frac{E_\sigma}{KT}) \qquad (2)$$

where σ_0 is the pre-exponential factor, K is Boltzmann constant and T is the absolute temperature

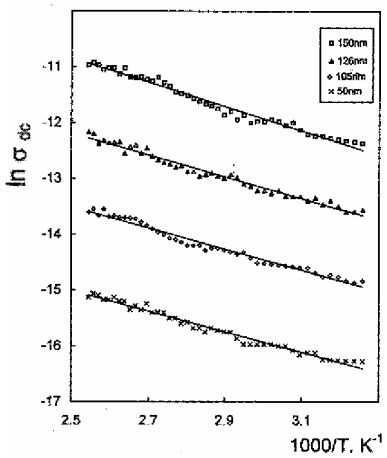

Fig. (3) Temperature dependence of dc conductivity σ_{dc} for $InSbTe_3$ thin films of different thicknesses

According to the Davis and Mott model [22] for the density of states of amorphous semiconductors, the value of the activation energy is expected to be smaller than half the optical energy gap by the width of the localized states E_e. Since E_g^{opt} =0.52eV and E_e=0.059eV as obtained below, so the expected value of the activation energy is ~0.201eV. The difference between the expected and the obtained mean value can be explained by a shift in Fermi level due to the inequality of positive and negative charge dangling bonds, observed in chalcogenide glasses [23,24].

3.3 Optical properties of $InSbTe_3$ thin films

The spectral distribution values of transmittance and reflectance for $InSbTe_3$ thin films of different thicknesses, measured in (25-150) nm range are shown in Fig. (4). The figures show that these films are transparent (T+R=1) in the wave length range (2100-2500) nm wavelength range. The spectral distribution of T and R for $InSbTe_3$ films measured in the (170-304) nm thickness range is shown in Fig. (5). From the figures it is observed that T+R<1 in the whole spectrum indicating that the films within this range of thickness posses absorption higher than the films in lower thicknesses (≤150nm). The reason of this behaviour may lie in true

 ISSN 1813-2065

wave length λ is represented as a function of the photon energy hυ and illustrated in Fig. (8).

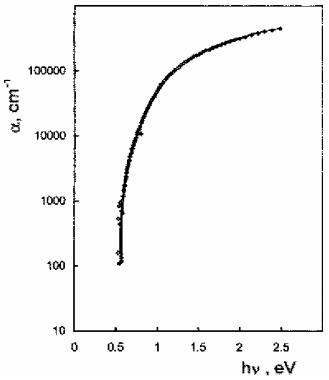

Fig. (8) Optical absorption coefficient (α) for $InSbTe_3$ thin films as a function of the photon energy *hv*

It is clear from this figure that the spectral distribution can be divided into two regions:
(i) The exponential edge region where $\alpha\nu<10^4 cm^{-1}$, where the Urbach [27] tail appears. In this region the absorption coefficient is governed by the relation [27]

$$\alpha(\nu) = \alpha_0 \exp\left(\frac{h\upsilon}{E_e}\right) \quad (3)$$

where E_e characterizes the band tail width

Therefore, plotting the dependence of [log α] as a function of *hv* should give a straight line as in Fig. (9), from which both α_0 and E_e can be evaluated ($\alpha_0=0.01 cm^{-1}$ and $E_e=0.055$eV).
(ii) For higher values of $\alpha\nu>10^4$ cm^{-1}, the variation obeys the relation [22]

$$\alpha(\nu) = A\frac{\left(h\nu - E_g^{opt}\right)^r}{h\nu} \quad (4)$$

where A is a constant, E_g^{opt} is the optical energy gap of the material and r is the number which characterizes the transition process

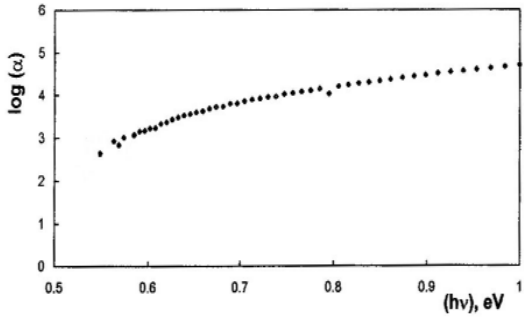

Fig. (9) Plots of log (α) as a function of *hv* for $InSbTe_3$ thin films

4. Conclusion

The dc electrical conductivity of $InSbTe_3$ thin films increases with increasing both thickness in the range (25-150nm) and temperature in the range (303-393K). Temperature dependence of dc electrical conductivity of thin films of

Optical constants for $InSbTe_3$ films with thicknesses in the range (25-150)nm range are determined from measured transmittance and reflectance by solving Murmann's [26] exact equations using graphical method which involves considerable computations as follows. A reasonable range is chosen for n and k within which both refraction and absorption indices are simultaneously increased in steps of 0.1 and 0.05 respectively. Using Murmann's exact equations, a set of curves representing transmittance and reflectance as a function of d/λ (d is the film thickness) are drawn for different values of n at constant k. Using these standard figures and for every value of transmittance and reflectance at a given wavelength, a new curves of $[k=f(n)]_{n \text{ from T}}$ and $[k=f(n)]_{n \text{ from R}}$ are drawn. The point of intersection of each set of two new curves yields the required values of n and k. The same method was repeated over the whole spectral region and for other films of different thicknesses.

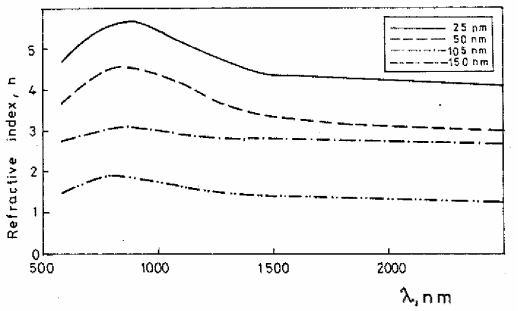

Fig. (6) Dispersion curves of refractive index *n* for $InSbTe_3$ films in the thickness (25-150) nm range

Hence the dispersion curves for n and k were obtained and illustrated in figures (6) and (7), respectively. It is indicated that the absorption index k is independent on film thickness in the considered range with an experimental error of ±2%, while the refractive index n decreases with increasing film thickness at any wavelength.

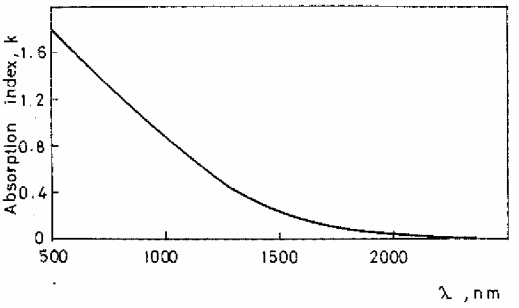

Fig. (7) Spectral distribution of absorption index (*k*) for $InSbTe_3$ in the thickness (25-150) nm range

The absorption coefficient (α) of $InSbTe_3$ thin films is calculated using the well known equation ($\alpha=4\pi k/\lambda$), in which k is the mean value of refractive index at each wavelength. The calculated values of α at different values of the

[7] M.A. Afifi et al., *Acta Physica Polonica*, 98(40) 401 (2000).
[8] A.M. Farid, H.E. Atyia and N.A. Hegab, *Vacuum*, 80, 284 (2005).
[9] M. Stordeur and G. Simon, *phys. stat. sol.*, (b) 124, 799 (1984).
[10] R. Sehr and L. R. Testardi, *J. Phys. Chem. Sol.*, 23, 1219 (1962).
[11] J. Horak, K. Cermak and L.Koudelka, *J. Phys. Chem. Sol.*, 42, 805 (1986).
[12] J. Horak et al., *J. Phys. Chem. Sol.*, 49, 191 (1988)
[13] J. Kroutil, J. Navratil and P. Lostak, *phys. stat. sol.*, (a) 131, K 73 (1992).
[14] P. Lostak et al., *phys. stat. sol.*, (a) 104, 841 (1987).
[15] V.A. Kulbachinskii et al., *Phys. Rev.*, B 52(15) 10915 (1995).
[16] H.E. Atyia and A.M.A. El.Barry, *Chalcog. Lett.*, 3(5) 41 (2006).
[17] L.Q. Men et al., *Proc. SPIE*, 2090, 82 (1996).
[18] J. Horak, S. Karamazov and P. Lostak, *Phil. Mag.*, B 72, 665 (1995).
[19] J. Horak, P. Lostak and L. Benes, *Phil. Mag.*, B 50, 665 (1984).
[20] M.A. Seyam and A. Elfalaky, *Vacuum*, 57, 31 (2000).
[21] L.K. Chopra, **"Thin film phenomena"**, Plenum Press (USA) (1969) 540.
[22] E.A. Davis and N.F. Mott, *Phil. Mag.*, 22, 903 (1970).
[23] H. Fritzsche and M. Kastner, *Phil. Mag.*, B 37, 285 (1978).
[24] N.F. Mott, *Phil. Mag.*, 34,1101 (1976).
[25] H.K. Pulker, *Appl. Opt.*, 18, 1969 (1979).
[26] M. Murmann, *Z. Phys.*, 101, 643 (1936).
[27] F. Urbach, *Phys. Rev.*, 92, 1324 (1953).

different thicknesses are nearly parallel lines in the considered ranges of thickness and temperature .This indicates that dc electrical activation energy ΔE_σ is single mean valued nearly independent on film thickness .Its mean value is 0.173 eV.

Optical constants *n* and *k* for $InSbTe_3$ amorphous thin films are determined from measurements of transmittance and reflectance in the wavelength range (400-2500nm). It is found that refractive index *n* decreases with increasing film thickness at any wave length, while absorption index *k* is practically independent on film thickness in the range (25-150nm). For films of thicknesses in the range (170-304nm), the spectral distribution of both T and R showed that T+R<1 in the whole spectrum. This is due to light scattering by surface roughness which is confirmed by electron microscope surface investigation. Analysis of the absorption index indicates that the absorption mechanism refers to the existence of optical indirect transitions with optical gap of 0.52 eV. The width of the tails of the localized states in the gap region is 0.055eV.

References

[1] C. Julien et al., *Thin Solid Films*, 137, 27 (1986).
[2] A.L. Zaslavskii, N.F. Kartenko and Z.A. Karachentseva, *Sov Phys. Solid State*, 13, 2152 (1972).
[3] G.L. Bleris et al., *phys. stat. sol.*, (a) 34, (1976) 243.
[4] M.A. Seyam, *Appl. Surf. Sci.*, 181, 128 (2001).
[5] A. Zahab, M. Abd-Lefdil and M. Cadene, *phys. stat. sol.*, (a) 11.7 K 103 (1990).
[6] N.A. Hegaab et al., *J. Mater. Sci.*, 33, 2441 (1998).

This article was reviewed at National Synchrotron Radiation Research Center, Taiwan, and School of Applied Sciences, University of Technology, Baghdad, Iraq

 ISSN 1813-2065

3DTV-CONFERENCE 2011-THE TRUE VISION CAPTURE, TRANSMISSION AND DISPLAY OF 3D VIDEO

16-18 MAY, 2011, Turkey

The 3DTV Conference, technically co-sponsored by IEEE, is becoming the premier forum for the presentation of research results and technological advances in relation to 3D television. 3DTV-CON 2011 will be the 5th conference of the series which originated from the EU FP6 3DTV Network of Excellence in 2006. Conference topics cover a wide range of fields including capture, processing, coding, transmission, visualization, interaction and applications of 3D TV.
Prospective authors are invited to submit four-page papers including results, figures and references. Papers will be accepted only by electronic submission. Detailed guidelines for submission will be provided in the 3DTV-CON 2011 website. The proceedings of the conference will be archived by IEEE Xplore, following the practice of the previous conferences. The main technical program will include several special sessions in emerging areas. Papers for special sessions will be accepted once the session topics are determined. In addition to the main technical program, there will also be tutorials and demonstrations/exhibitions. Proposals for special sessions, tutorials and demonstrations/exhibitions should be submitted to the appropriate chair(s).

3D Capture and Processing

- 3D capture and reconstruction for static and dynamic scenes
- Design and implementation of novel camera systems
- Multi-modal sensor data processing for 3D reconstruction and tracking
- Mixing of virtual and real worlds
- 3D head pose and gaze tracking
- Signal processing for diffraction and holographic 3DTV

3D Coding and Transmission

- Novel systems and architectures for 3DTV transmission
- Multi-view video coding
- Compression of depth and dispariy maps, meshes, holograms, and light fields
- Error resilience and concealment techniques
- Audio coding for 3DTV
- Advances in quality of service

3D Visualization and Interaction

- Stereoscopic and auto-stereoscopic display techniques
- Holographic display technology, integral imaging techniques
- Underlying optics and VLSI technologies
- Novel representation techniques for 3D data
- Novel forms of interaction with 3DTV
- Human factors and health effects of 3D vision

3D Applications

- 3D television, cinema, and games
- 3D tele-immersion and remote collaboration
- Augmented and virtual reality environments, virtual heritage and virtual archaeology
- Medical and biomedical applications
- 3D digital signage
- 3D content-based retrieval and recognition

Tentative Submission Deadline: 15 December 2010

Homepage: http://www.3dtv-con.org/3dtv-con-11/d2/index.php

Lu Y. Zhao
Yang M. Ming
Li W. Lang
Qiuming Yao

Department of Physics,
Renmin University of China,
59 Zhongguancun Ave,
Beijing, 100872, China

Field Dependent Critical Trap Density for Thin Gate Oxide Breakdown

We have found that the total trapped negative charge in a thin gate-oxide at the point of breakdown is a strong function of the stress field. This observation is in direct contrast with previous reports in the literature. The field dependent behavior of total trapped charge leads to the conclusion that the critical trap density for breakdown is also field dependent. We use the field dependent hopping conduction to explain why the critical trap density for breakdown in the percolation model should be field dependent.

Keywords: Trap density, gate breakdown, Thin oxide, Field dependency
Received: 11 September 2010, **Accepted**: 26 October 2010

Introduction

Because of the importance of thin gate oxide in silicon integrated circuits, its reliability, particularly its breakdown behavior has been studied intensively by many groups for many years. Yet, a clear physical mechanism still eludes us. Recently, the percolation model of oxide breakdown has evolved and gained wide acceptance [1-7]. According to this model, traps are created in the oxide during electrical stress and, when the density of traps reaches a critical value, breakdown occurs. While this model does not say anything about the microscopic nature of the traps that are responsible for breaking down the gate oxide, Degraeve et al [7] managed to extract from it an effective radius of the traps. This kind of information is highly valuable in the construction of a physical model of oxide breakdown.

It is believed that since the nature of trap does not change with gate oxide thickness or oxide field, the critical trap density of a given type of oxide sample is fixed [7]. Based on this idea, the field dependent charge to breakdown (Q_{BD}) for an oxide is simply the result of reaching the same critical trap density with a different (field dependent) trap generation rate [7, 11]. Thus, if the trap generation rate can be measured, one can predict Q_{BD} without actually carrying out the breakdown test [8]. Such approach, if it works, will significantly reduce the testing time as well as sample size for gate-oxide reliability assessment.

In this paper, however, we report experimental evidence that the critical electron trap density is dependent upon the applied field.

Experiment

Our samples are $2.3 \times 10^{-4} cm^2$ capacitors with 52Å thick gate-oxide grown by dry oxidation at 850ºC. The gate electrode is n+ tungsten-polycide with aluminum metal on top. All stresses were constant current in gate injection mode (gate negative). All oxide failures were hard breakdowns. Figure (1) shows the Weibull plot of Q_{BD} for four different stress current densities. As expected, higher stress leads to lower Q_{BD}. In our measurement, the entire time history of the gate voltage required to maintain the constant current is recorded. An example of such a record is shown in Fig. (2).

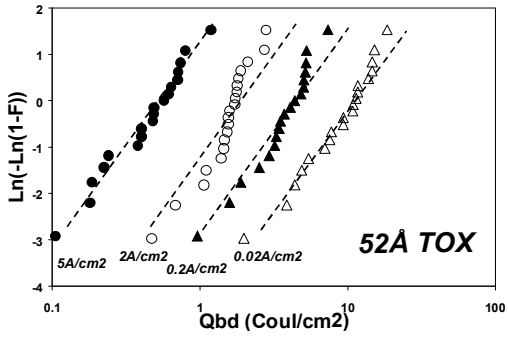

Fig. (1) Weibull distributions of Q_{BD} for 4 constant current stress levels. Dotted lines are guide for the eye only

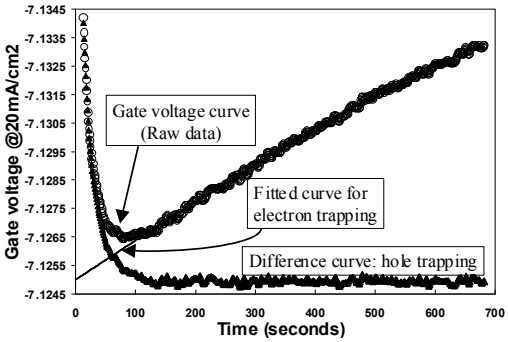

Fig. (2) Time record of gate voltage needed to maintain constant current and the separation of electron and hole trapping

The turn-around behavior of the gate voltage versus time curve (raw data) is well known [9]. The initial rapid decrease in gate voltage is due to efficient hole trapping [12]. Hole trapping reaches steady state (levels off) rapidly and, as a result, the change in gate voltage after the 'turn around' is due entirely to electron trapping. One can therefore fit this part of the curve with a polynomial and extrapolate back to time zero as shown in figure 2. This fitted curve represents the entire time history of gate voltage change due to electron trapping alone. From the time zero gate voltage of the fitted curve and the gate voltage at breakdown, we obtained the total ΔV_G due to electron trapping for each stressed sample. The total trapped negative charge Q_T at time of breakdown can thus be calculated using

$$\Delta V_g = \frac{Q_T(t_{ox} - x)}{\varepsilon t_{ox}} \quad (1)$$

Here x is the charge centroid (measured from the gate/SiO_2 interface) of the negative trapped charges (not the centroid of the total trapped charges). t_{ox} is the gate-oxide thickness. Assuming a uniform trap distribution (a reasonable assumption for gate-oxide this thin), x is simply $t_{ox}/2$. If the trap distribution is non-uniform, the calculated Q_T will be off by a small factor. As long as the charge centroid does not vary much going from 11 to 14 MV/cm of stress field, the correction factor is approximately constant. Therefore, the fact that we do not know the actual trapped charge distribution does not affect the conclusion.

Figure (3) shows the plot of Q_T versus Q_{BD} for all the stressed samples. Since Q_T and Q_{BD} are extracted from the same sample, each group of capacitors shows a well-behaved relationship as expected. This relationship, as seen from the figure, is very close to a straight line. The power law relationship between Q_T and Q_{BD} reported by Vincent et al [11] is not observed.

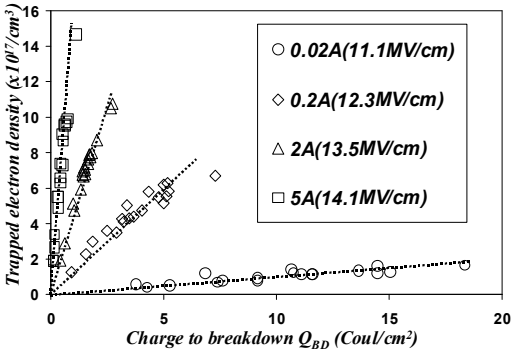

Fig. (3) Trapped electron density Q_T vs. Q_{BD} for the 4 stress populations

The most unexpected result shown in figure 3 is that Q_T population for higher stress field has significantly higher value than the Q_T population for lower stress field. If the critical trap density is independent of stress field, one expects the Q_T population for higher stress field to be lower, not significantly higher as observed. The reason for expecting a lower Q_T is that field induced detrapping is more efficient at higher field. A lower filling factor (fraction of traps occupied by electrons) is therefore expected [7, 13].

An obvious possibility for the observed higher Q_T at higher field is that, even though the filling factor decreases with field at lower field, it turns around and increases drastically with field at higher field. Such assumption implies that at higher field, either the efficiency of detrapping decreases rapidly or the trapping efficiency increases rapidly. Our data cannot exclude either possibility. The possibility of detrapping efficiency decreases at higher field is counter-intuitive to the picture of detrapping being a field assisted tunneling of trapped charge out of the oxide. There is no reason to expect a turn around behavior for the detrapping process. On the other hand, it is possible that the trapping efficiency increases rapidly at higher field. If this is the case, it has important implications for the trapping mechanism.

Vincent et al [11] found that the total trapped charge (predominantly electrons) at breakdown is independent of the stress current (and thus the stress field). However, their measurement was done only on one sample per stress condition. Even for the same stress condition, a wide range of charge to breakdown is expected as is evident in figure 3. A conclusion drawn from single observation per stress condition is not reliable.

DeGraeve et al [7] used a trap filling technique to measure the trap density after stress. They too found that the trap density at breakdown is independent of field. However, they too suffer from the problem of a small number of samples. Both groups employed the method of stress and measure at various points in time for each sample. This method is time consuming and is probably the reason for the very small number of samples studied. The method of Vincent further suffers from the problem of detrapping during the time between stress and measure as well as during measurement. Such uncontrolled detrapping increases the uncertainty of the measured results. DeGraeve et al did not cover the higher field range reported here. Their measurements were all done at fields below 11MV/cm. Imagine, for a moment, that in figure 3, another set of data at a lower field is plotted. This new set of data is expected to follow a line below that of the 11.1MV/cm data set. Assuming it has similar scatter as the sets of data in Fig. (3), it is clear that the new set will mix with the 11.1MV/cm set in most places. When the data set is large, it is entirely possible to plot a distinct line of smaller

slope through the new set. When the data set is only a couple of points per field condition, it will be impossible to detect the field dependent behavior.

Our measurement method is unique in that it completely separated the effect of hole trapping from electron trapping. Our measurement is done during stress, not afterward, and therefore free from the problem of uncontrolled detrapping. It is also very efficient so that large number of samples can be studied.

Discussions

If we take the most apparent explanation for the observed result of figure 3, that is, the critical trap density increases with the applied field, what reason would one have for that to be true?

Exactly what the conduction mode is at the point of gate-oxide breakdown before thermal run-away is still not known. Okada [14] used the $T^{1/4}$ dependent of the "B-mode SILC" (soft breakdown) to argue that the conduction mode is variable range hopping. Since the defects that cause breakdown to occur are expected to be very deep traps, hopping can only occur via phonon assisted tunneling. Given the expected size of the breakdown spot (~100Å^2) and the expected tunneling distance of 9Å (4.5Å effective trap radius), it is hard to explain the level of current (10^{-8} to 10^{-6} amp) observed at soft breakdown. Translating into current density, the post soft breakdown current is in the range of 10^6 to 10^8 A/cm^2, too high for a tunneling process.

Cheung et al [15] proposed a model of conduction through delocalized electron wave in defect band, which can explain the highly conductive state after breakdown. However, before reaching such a state, hopping must be the conduction mechanism. Accordingly, we expect gate-oxide breakdown without thermal run-away to be a two step process: the formation of a most efficient hopping conduction path and the change of conduction mode by creating more traps along the path due to the sudden increase in electron flux. This is not the thermal run-away process because the oxide remains only soft-broken.

If hopping is the conduction mechanism all the way up to the formation of the conduction path, we must then seek answer to the field dependent critical trap density puzzle in the effect of an applied field on hopping. Fortunately, the problem of hopping conduction in the presence of an applied field for a disordered system is well established. One of these studies was by Apsley et al [10].

Figure (4a) shows a typical picture for breakdown for the critical electron trap density model. Here we deliberately show that the linking of traps can go backward against the force due to the applied field F. Such cases are allowed in the percolation model. In the presence of an applied field, the backward hop becomes a high resistance link (Fig. 4b). A conduction path is not formed. When the F is small, the probability difference between forward hop and sideways hop is negligible. However, as F increases, the probability for a forward hop is very much higher than a sideways hop. In other words, in the presence of an applied field, all hops other than forward are negligible.

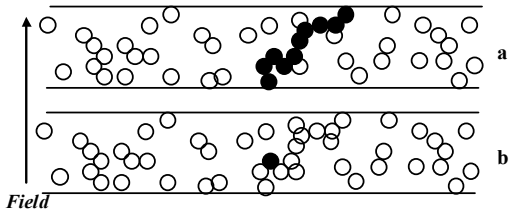

Fig. (4) (a) Breakdown by linking traps together in critical electron trap density model, (b) When an applied field exist, conducting backward is not allowed (blacken circles)

Instead of the linkage shown in figure 4, a more line-up linkage is needed for breakdown as shown in Fig. (5). Since the more line-up linkage is a subset of all possible linkages, the probability for it to happen at a given trap density is lower. Thus the critical trap density must go up with the field.

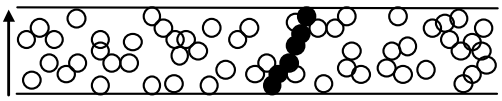

Fig. (5) At high field, the direction of conduction forces a prefer direction for the traps to link up to produce a breakdown

Just how much is a backward hop suppressed by the external field? We can estimate that following Apsley et al's approach. The phonon assisted hopping probability in a disordered system is [10]:

$$P_0 \propto \exp\left(-2\alpha R - W/kT\right) \qquad (2)$$

Where α^{-1} is the attenuation length of the localized electron wave function. R is the hopping distance. W is the energy separation of the initial and final state, which is the phonon energy in the phonon-assisted tunneling. When an external applied field exists, the hopping probability become direction dependent. Let θ be the angle between the hopping and the applied field (Fig. 6)

The hopping probability changes to:

$$P \propto \exp\left(-2\alpha R - \frac{\left(W - qFR\cos\theta\right)}{kT}\right) \qquad (3)$$

ISSN 1813-2065

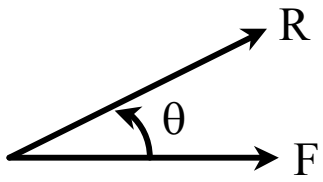

Fig. (6) Angle between hopping direction and applied field direction

Combining the equations with and without field, we can get the expression to calculate the impact of applied field on hopping probability:

$$\ln\left(\frac{P}{P_0}\right)=\frac{qFR\cos\theta}{kT} \qquad (4)$$

and at room temperature, kT/q=25.8mV

If we take R to be 9Å [7], one can calculate $\log(P/P_0)$ as a function of field and angle. Figure (7) shows the result.

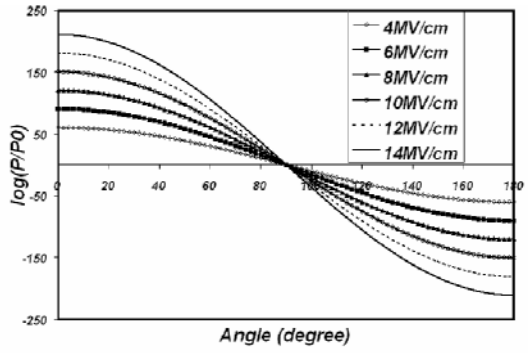

Fig. (7) Hopping probability change as a function of angle between applied field and hopping direction

As can be seen, the impact of a high external field on hopping probability is huge. The difference in probability between exactly forward and exactly backward hopping at 14MV/cm is over 400 orders of magnitude (for the 9Å hopping distance case). At first glance, the magnitude of the probability change seems unreasonably large. In reality, it is actually quite normal to expect such a large change in tunneling probability. Going from 0-degree angle to 90-degree angle in Fig. (7) changes the field in the hopping direct from 14MV/cm to zero. If we take the familiar Fowler-Nordheim tunneling equation of

$$J = AF^2\exp\left(\frac{-B}{F}\right) \qquad (5)$$

where A=1.25x10^{-6} and B=233.5 and plot the tunneling current for the full range of field, we see that the tunneling probability changes by more than 300 orders of magnitude going from 14MV/cm to zero field (Fig. 8).

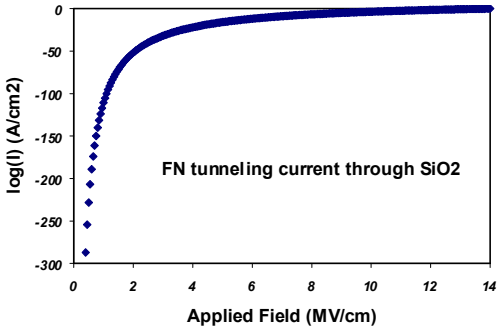

Fig. (8) Fowler-Nordheim tunneling current density through SiO_2 as a function of applied field

It is clear from Fig. (7) that even if there is a site that is very close by to hop to, if it is in the wrong direction, the hopping would be to a farther site that is in line with the applied field. It is obvious that the case considered in Fig. (4) never occurs. All breakdowns must involve forward hopping path only. In fact, all breakdown paths must be quite similar to the one in Fig. (5). The breakdown model that allows random direction of the critical conduction path must be modified to include constraints on the hopping direction.

If all breakdown paths are fairly in line with the applied field, then where does the field dependence of the critical trap density come from? It comes from the degree of straightness of the breakdown path. Even at small angle, the influence of the applied field is still very strong. Figure (9) shows the effect of field on hopping probability as the hopping direction deviates from 0-degree. It is shown as the decrease in hopping probability as a function of increasing angle.

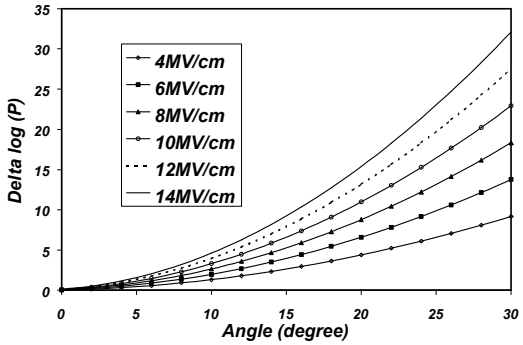

Fig. (9) The hopping probability changes as a function of the angle and field

As the field increases, the acceptable angle for the formation of breakdown path decreases. The increase in constraint means reduction in the probability of the formation of such path at a given trap density. Conversely, the increase in constraint means an increase in critical trap density for breakdown to occur.

For each field strength, there exists an angle below which further decrease in angle produces a

probability change smaller than the impact of the initial and final state energy difference. Within that critical angle, the impact of the applied field diminishes. Since the initial and final state energy difference is determined by the phonon energy, it can be represented in Fig. (9) as a fixed probability. If we pick a fixed probability decrease as the point below which the angle no longer important and plot that angle as a function of field, we find a saturation behavior as shown in Fig. (10). Note that the point of fixed probability decrease in Fig. (10) was picked arbitrarily to illustrate the saturation behavior. It should not be taken as a meaningful quantity.

If the acceptable angle as a function of field saturates, so should the critical trap density. This is indeed the case as shown in Fig. (11), from which we see that at 11MV/cm, the median Q_T is $1.3x10^{17}/cm^3$. Degraeve et al [7] reported a 3% filling factor at 7MV/cm. Using the same value, we calculate the median critical trap density to be $4x10^{18}/cm^3$. This value is somewhat smaller than those reported in Ref. [7] for similar field and oxide thickness (after area correction). Thus, our assumption that the filling factor continues to decrease with field is valid at least at 11MV/cm.

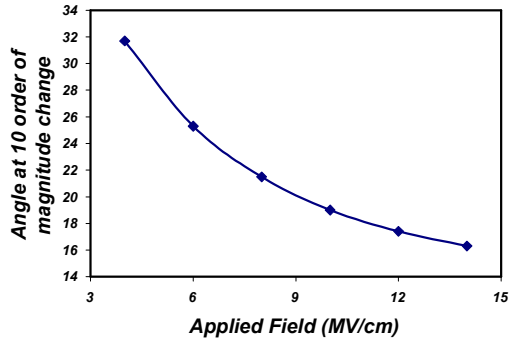

Fig. (10) For a fixed probability change, the reduction of acceptable angle as a function of field saturates

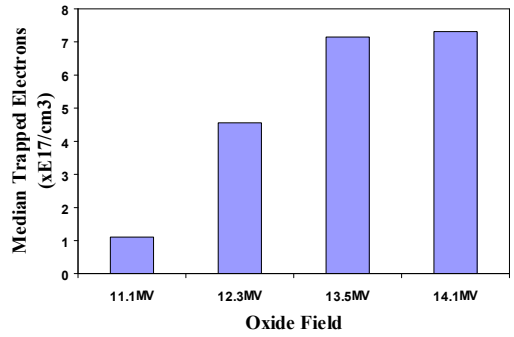

Fig. (11) Median QT as a function of oxide field in MV/cm

Conclusions

Using a more efficient and accurate method to measure trapped negative charge in the gate oxide at the point of breakdown, we found that, contrary to previous reports, the total trapped charge is dependent on the applied field. We argue that this is due to a field dependent critical trap density for breakdown. This finding represents a significant departure from the current widely accepted model. We presented physical arguments to support the field dependency of critical trap density. The key factor involve is the effect of an external applied field on the probability of phonon assisted hopping conduction. Qualitatively, our data agrees with the physical model. Our result extended the current model of breakdown for gate-oxide. As a result, the statistical simulation of Ref. [7] must be redone to find a new effective trap radius.

References

[1] J. Suñé et al., *Thin Solid Films*, 185, 347(90).
[2] N. Shiono and M. Itsumi, *Intl. Relib. Phys. Symp.* IRPS (1993) 1.
[3] H. Satake and A. Toriumi, *Intl. Eelectron Device. Meet.* IEDM (1993) 337.
[4] P.P. Apte and K. C. Saraswat, *IEEE Trans. Electron Dev.*, 41(9) (1994) 1595.
[5] D.J. Dumin et al., *Intl. Relib. Phys. Symp.* IRPS (1994) 143.
[6] D.J. DiMaria and H.J. Stathis, *Appl. Phys. Lett.*, 70(20) (1997) 2708.
[7] R. Degraeve et al., *IEEE Trans. Electron Dev.*, 45 (1998) 904.
[8] K. Okada et al., *Proc. VLSI Technolog. Symp.*, (1998) 158.
[9] K.P. Cheung, *IEEE EDL,* 15(11) (1994) 460.
[10] N. Apsley and H. P. Hughes, *Phil. Mag.*, 30 (1974) 963.
[11] E. Vincent, C. Papadas and G. Ghibaudo, *Proc. ESSDERC*, (1996) 765-770.
[12] Y. Nissan-Cohen, J. Shappir and D. Frohman-Bentchkowsky, *J. Appl. Phys.*, 54(10) (1983) 5793.
[13] Y. Nissan-Cohen, J. Shappir and D. Frohman-Bentchkowsky, *J. Appl. Phys.*, 60(6) (1986) 2024.
[14] K. Okada and K. Taniguchi, *Appl. Phys. Lett.*, 70 (1997) 351.
[15] K.P. Cheung et al., *Tech. Digest 1997 Symp. VLSI Technol.*, 145.

This article was reviewed at Department of Chemistry, Middle East Technical University National, Turkey, and School of Applied Sciences, University of Technology, Baghdad, Iraq

 ISSN 1813-2065

International Conference on Applied Physics and Mathematics (ICAPM 2011)
April 29-30, 2011, India

International Conference on Applied Physics and Mathematics (ICAPM 2011) is the premier forum for the presentation of new advances and research results in the fields of theoretical, experimental, and applied Physics and Mathematics. The conference will bring together leading researchers, engineers and scientists in the domain of interest from around the world.

Topics of interest for submission include, but are not limited to:

Advanced Numerical Algorithms
Algorithmic Approaches to Computational Kernels and Applications
Application of Soft Computing, Knowledge Engineering, and Machine Learning
Applications of Computation as a Scientific Paradigm
Artificial Intelligence and Soft Computing (Neural, Fuzzy, Evolutionary Systems)
Automation, Control and Robotics
Aviation & Space Technology
Bioengineering and Bioinformatics
Biomedical Physics and Engineering
Boundary Element Methods
Circuits, Networks and Systems
Complex Systems: Modeling and Simulation
Computation in Complex Networks
Computational Science and Engineering
Computational Mathematics
Computational Mechanics, Economics, Finance and Statistics
Computational Physics, Chemistry, Biology and Medicine
Computational Statistics
Control of Dynamical Systems
Dynamical Systems
Electronics, Microelectronics and Nanoelectronics
Engineering Mathematics
High Performance Computing
Hybrid Computational Methods
Industrial Mathematics
Instrumentation and Measurement
Materials Science
Mathematical Methods in Sciences and Engineering
Mathematical Modeling
Mathematical models for the information society
Mathematical models in Economy and Insurance
Mathematical models in Medicine
Mechanics and Fluid Mechanics
Meshless Methods
Multimedia and Video Systems
Nonlinear Analysis
Numerical Techniques
Optimization Inverse Problems
Parallel and Distributed Computing
Parallel Numerical Algorithms
Parallel Processing in Computational Mathematics
Pattern Recognition and Image Analysis
Power Systems
Problem Solving Environments
Robotic Technologies
Scientific Computing
Signal Processing, Speech Processing, Image Processing
Simulation and Gaming
Software Tools
Solving ODE and PDE Models
Systems Theory, Dynamical Systems, Chaos
Telecommunication Systems
Visualization and Virtual Reality
Web and Grid-based Simulation and Computing
Web, IT-based Computer-aided Engineering

The ICAPM 2011 conference proceeding will be published by IEEE, which will be included in the IEEE Xplore, and indexed by the Ei Compendex, ISI Proceeding and other indexing services.

Important Date

Paper Submission (Full Paper) Before December 20, 2010
Notification of Acceptance On January 20, 2011
Final Paper Submission Before February 10, 2011
Authors' Registration Before February 10, 2011
ICAPM 2010 Conference Dates April 29 - 30, 2011

Tentative Submission Deadline : 20 December 2010

Homepage: http://www.icapm.org/cfp.htm

Rafid K. Kadhum
Tariq S. Salman
Suhad A. Mahmood

Department of Materials Engineering, College of Engineering, Universityof Babil, Hilla, Babil, Iraq

Modeling of Temperature-Dependent Absorptivity of Laser-Treated Surface

In this work, we have considered the effect of the various properties on the thermal field, the absorptivity plays a special role, because it controls directly the heat input to the sample, while being itself a function of surface temperature. In order to take this dependence into account, the one-dimensional heat conduction equation was solved for a semi-infinite geometry using variable absorptivity and assuming constant thermal conductivity and thermal diffusivity. It is shown that the surface temperature satisfies an Abel integral equation with an approximate analytical solution that gives a temperature rise at the surface linear with t. Comparison is made between analytical approximate expressions, numerical solutions, previous models and experimental results.

Keywords: Absorptivity, Laser treatment, Melting threshold, Surface temperature
Received: 20 May 2010, **Revised**: 12 September 2010, **Accepted**: 19 September 2010

Nomenclature

α thermal diffusivity, $m^2\ s^{-1}$
χ temperature coeff. of electrical resistivity, K
δ optical absorption depth of laser radiation, m
ε_O permittivity of vacuum, $C^2.N^{-1}.m^{-2}$
λ wavelength of laser radiation, m
ρ electrical resistivity, Ω.m
ρ_O electrical resistivity at room temperature, Ω .m
A absorptivity (A = 1 - R, R: reflectivity)
c velocity of light in vacuum, $m\ s^{-1}$
I power density, $W.m^{-2}$
J_m energy density (melting threshold), $J.m^{-2}$
K thermal conductivity, $W.m^{-1}.K^{-1}$
L thickness of sample, m
r beam radius, m
T temperature, K
T_O surface temperature, K
t time, s
t_p pulse duration, s
x distance to surface, m

1. Introduction

During the last three decades, lasers have been widely used for materials processing. Since many applications rely on the thermal effects of laser-material interaction, it becomes very important to obtain information about the temperature field as a function of processing parameters and materials properties. For that purpose, several models have been proposed, both analytical and numerical. Despite the fact that extremely sophisticated numerical models have become available, analytical expressions continue to be used. This is often due to simplicity and also because they allow to obtain simple relations between the process parameters that give a better insight on the phenomena involved.

In some cases, analytical models can take into account the fact that parameters affecting the thermal field depend themselves on temperature. For instance, the Kirchoff Transform [1] is performed to account for the dependence of thermal conductivity on temperature. Nevertheless, for many materials, the variable which more strongly affects the final result is the absorptivity, because it controls directly the amount of energy that is transferred into the material. Considering that the absorptivity varies linearly with temperature, a one-dimensional model was proposed by Sparks and Loh [2].

However, the dependence of absorptivity on temperature can be expressed in a different way by means of Hagen-Rubens equation [3, 4], in which A is expressed as a function of the wavelength of radiation and the electrical resistivity of the material. The main goal of the present paper is to present an analytical expression for the surface temperature of a laser irradiated material in which the variation of absorptivity with temperature follows Hagen-Rubens equation. The heat conduction regime will be considered as one-dimensional, an approximation that is valid when the characteristic heat conduction distance is negligible as compared to the diameter of the laser beam. Moreover, we will apply the present analysis to the estimation of pulse duration

 ISSN 1813-2065

leading to melting on the surface of a laser irradiated material, for constant power density.

In laser surface treatment of materials, it is a matter of practical importance to determine relations combining the various processing parameters. For a particular laser setup and for a certain practical requirement, such a relation is quite useful for the purpose of process optimisation. For instance, in pulsed laser irradiation, when the requirement is that a definite value of temperature is attained at the surface (e.g. the melting temperature), a relation between power density and pulse duration should be looked for. If heat conduction is one-dimensional and the material properties are considered as temperature independent, a first estimate can be done by using a simple analytical model, which gives a temperature rise at the surface proportional to $t^{1/2}$.

2. Assumptions

We will develop our model based on the following assumptions:

a) $r >> 2\sqrt{\alpha t}$ $\Rightarrow$ one-dimensional heat conduction.

b) $L >> 2\sqrt{\alpha t} \Rightarrow$ semi-infinite solid.

c) $\delta << \sqrt{\alpha t_p}$, $\Rightarrow$ surface heating.

d) The surface is polished and clean.

e) The thermal conductivity and thermal diffusivity are taken as constants.

f) The electrical resistivity varies linearly with temperature.

g) The absorptivity varies with temperature according to Hagen-Rubens equation.

h) The laser pulse shape is square.

3. Leading equations

For one-dimensional heat conduction with constant thermal properties and semi-infinite geometry we write:

$$\frac{\partial T}{\partial t} = \alpha \frac{\partial^2 T}{\partial x^2}, \qquad 0 \le x < \infty \tag{1}$$

The initial and boundary conditions are:

$$T(x,t=0) = 0 = T(x=\infty,t) \tag{2}$$

$$-K \left.\frac{\partial T}{\partial x}\right|_{x=0} = A\big(T(x=0,t)\big) I \tag{3}$$

We consider the Hagen-Rubens law [3] (which gives good agreement with experimental values for the absorptivity of various metals when $\lambda > 5$ μm [4]):

$$A = 2\sqrt{\frac{4\pi\varepsilon_o c\rho}{\lambda}} = 0.365\sqrt{\frac{\rho}{\lambda}} \tag{4}$$

which is the first term of Bramson's equation [4]. We assume that the electrical resistivity varies linearly with temperature:

$$\rho(T) = \rho_o \left(1 + \frac{T}{\chi}\right) \tag{5}$$

4. Solutions

The solution for the surface temperature can be obtained by applying the Duhamel theorem [1]. The result is:

$$T_o(t) = \frac{\eta E}{2} \int_0^t \sqrt{\frac{T_o(s) + \chi}{t - s}}\ ds \tag{6}$$

with:

$$E \equiv \frac{2I}{K}\sqrt{\frac{\alpha}{\pi}} \tag{7}$$

and:

$$\eta \equiv 2\sqrt{\frac{4\pi\varepsilon_o c\rho_o}{\chi\lambda}} \tag{8}$$

which is an integral Abel equation. An exact solution for the case $\chi = 0$ and finite η can be found:

$$T_o(t) = \mu t \tag{9}$$

with:

$$\mu \equiv \left(\frac{\pi\eta E}{4}\right)^2 \tag{10}$$

which we will refer to as the linear solution.

4.1 Adimensional Variables

We introduce now a characteristic time:

$$t^* = \frac{\chi}{\mu} \tag{11}$$

Adimensional temperature and time can be defined, respectively, as:

$$\varphi_o \equiv \frac{T_o}{\chi} \tag{12}$$

$$\tau \equiv \frac{t}{t^*} \tag{13}$$

By doing so, we obtain an Abel equation independent on materials properties:

$$\varphi_o(t) = \frac{2}{\pi} \int_0^\tau \sqrt{\frac{\varphi_o(s) + 1}{\tau - s}}\ ds \tag{14}$$

The linear approximate solution can now be written as:

$$\varphi_o(\tau) = \tau \tag{15}$$

By introducing this expression into the RHS of Abel equation, a more accurate analytical solution is obtained, still in a closed form:

$$\varphi_o(\tau) = \frac{2}{\pi}\left[\sqrt{\tau} + (1+\tau)\ arctg\left(\sqrt{\tau}\right)\right] \tag{16}$$

which will be referred to as the approximate analytical solution. Note that this expression

tends to the linear solution (15) when $\tau >>1$. Also, for $\tau << 1$, equation 16 can be written as:

$$\varphi_o(\tau) = \frac{4}{\pi}\sqrt{\tau} \qquad (17)$$

which is the well known Carslaw and Jaeger solution [1] for constant materials properties, with absorptivity taken at room temperature.

5. Results and Discussion

Calculations were made to obtain the adimensional surface temperature as a function of adimensional time for laser irradiation of copper (figure 1) and aluminum (figure 2). In both figures we display the results for:

a) equation 15 (linear solution);
b) equation 16 (approximate analytical solution);
c) numerical solution of Abel equation (14);
d) numerical solution of the heat conduction equation taking K, α and A as temperature dependent;
e) Carslaw and Jaeger solution (equation 17);
f) Sparks and Loh equation [2];
g) experimental value of melting threshold energy density for a 100 ns pulse of 10.6 μm laser radiation [2, 5]. An adimensional pulse duration was calculated as:

$$\tau_p = \frac{\pi \rho_o \alpha}{t_p \lambda}\left(\frac{0.365 J_m}{2\chi K}\right)^2 \qquad (18)$$

h) adimensional melting temperature.

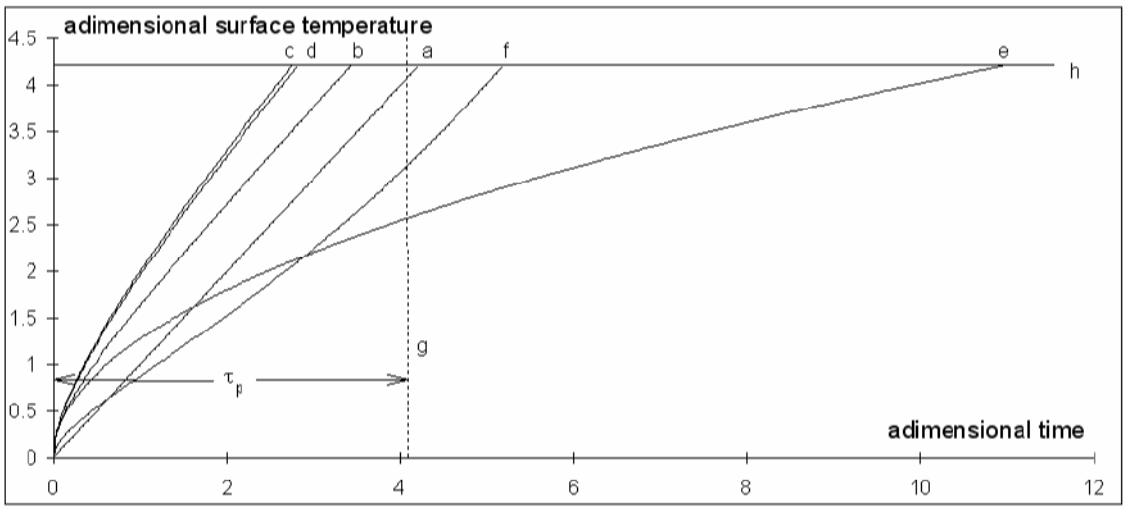

Fig. (1) Results for copper. Data from references [2, 6, 7]. Curves a-g: see text

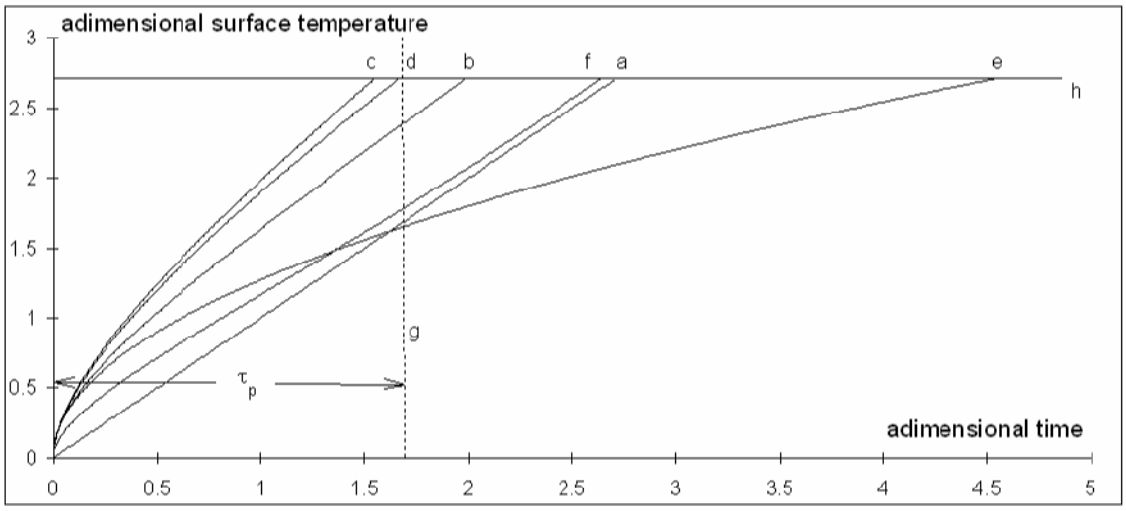

Fig. (2) Results for aluminum. Data from references [2, 6, 7]. Curves a-g: see text

The experimental values for adimensional melting temperature and adimensional pulse duration are represented by horizontal and vertical lines, respectively, for better comparison with the results obtained by the models a-f.

ISSN 1813-2065

We see that the approximate (a) and the linear (b) solutions match well the experimental results (g), in contrast to Carslaw and Jaeger expression (e). Solutions (a) and (b) predict values for the pulse duration similar to those obtained by numerical calculations (c) and (d) and also to the results of Sparks and Loh (f), yet showing greater simplicity.

We see in both cases that temperature dependence of the thermal properties also influence the results, but not as much as the absorptivity. So, the linear solution gives a particularly simple way of estimating melting thresholds, avoiding large errors that usually arise using the constant absorptivity approximation.

6. Conclusions

An integral Abel-type equation independent on material properties was derived. Its numerical solution can be used to obtain the surface temperature of a laser irradiated material with temperature dependent absorptivity following Hagen-Rubens equation, in good agreement with experimental results. Simple analytical solutions were obtained, giving also a reasonable estimation of melting thresholds. The analytical formulae give results which are similar to Sparks and Loh's, yet showing the following advantages: simplicity and electrical resistivity data is widely available.

References

[1] H. Carslaw and J. Jaeger, **"Conduction of Heat in Solids"**, 2nd ed., Oxford University Press, Oxford. (1959) 10,30,75-76.

[2] M. Sparks and E. Loh, Jr., *J. Opt. Soc. Am.*, 69(6) (1979) 847.

[3] E. Hagen and H. Rubens, *Über Beziehungen des Reflexions- und Emissionsvermögens der Metalle zu ihrem elektrischen Leitvermögen*, *Annln. Phys.*, 11 (1903) 873.

[4] M. Bramson, **"Infrared Radiation"**, Plenum Press, New York (1968) 127.

[5] J.O. Porteus, M.J. Soileau and C.W. Fountain, *Appl. Phys. Lett.*, 29 (1976) 156.

[6] Y.S. Touloukian *et al.*, **"Thermophysical Properties of Matter"**, IFI/Plenum, New York, vol. 1 (1970); vol. 4 (1970); vol. 10 (1973).

[7] J.R. Davis *et al.*, **"Metals Handbook"**, vol. 2, 10th ed., ASM International, USA (1990).

This article was reviewed at Department of Applied Physics, University of Vigo, Spain, and School of Applied Sciences, University of Technology, Baghdad, Iraq

---

Ayham M. Ali
Namir A. Jasim

Department of Electrical Engineering, University of Mosul, Mosul, Iraq

Studying Defects on Semiconductor Surfaces by Photoacoustic Spectroscopy

This paper presents both theoretical and experimental issues connected with measurements and numerical analysis of the microphone amplitude and phase photoacoustic spectra of semiconductor samples exhibiting surface absorption connected with defects states located on their surfaces. The analytical model of surface absorption in semiconductors is described and the results of computations are compared with experimental amplitude and phase spectra for $Zn_{0.965}Be_{0.035}Se$ crystal samples. This paper shows the importance of the phase spectra for the proper interpretation of the PA (photoacoustic) results.

Keywords: Photoacoustics, Surface defects, Semiconductors, ZnBeSe structure
Received: 13 July 2010, **Revised**: 18 August 2010, **Accepted**: 25 August 2010

1. Introduction

In recent years the Photoacoustic Spectroscopy (PAS) has extended even further its capability for materials characterization, as for instance in nanosized materials [1]. In this study we report on the room-temperature PAS investigation of hidrogeochemical and hydrological samples composed of precipitation water (Prec), groundwater (GW), through flow water (TF), overland flow water (OF), and stream flow water (SW) [2,3]. Our investigation of the collected samples using PAS was supported by pH evaluations and conductivity measurements. Several techniques, such as hidrochemical analysis [2] and chromatography [3], have been recently used in the investigation of the environmental impact caused by slash and burn agricultural practices [2]. Particle induced X-ray emission was used to quantify the concentration of elements whereas a large study of aerosol and trace gas properties was conducted in the Amazon region during the dry and wet seasons, for pasture and primary forest sites, as a way to evaluate traces of the nitric oxide, nitrogen dioxide, ozone, carbon oxide, and carbon dioxide among others [4]. However, the increasing interest in the understanding of the environmental dynamic changes occurring in the Amazon region requires the use of alternative spectroscopic techniques for environmental diagnosis and monitoring, especially those applicable to the molecular dynamics at the periods comprising the transition from wet to dry and from dry to wet seasons [5]. Particularly interesting are experimental techniques, capable of run *in situ* diagnosis and monitoring, as PAS is expected to provide. PAS is a well-established experimental technique [6], with a wide range of applicability in materials science.

Photoacoustic spectroscopy with a microphone detection was applied in the past for investigations of the optical properties of semiconductors. In the most common approach the numerical analysis of the photoacoustic (PA) spectra is performed in a previous study [7] that enables computation of the optical absorption coefficient spectrum from the PA amplitude spectrum. This approach has however some essential limitations: it is correct for thermally thick samples and it was derived in the model of a volume absorption. Because of the simplicity of the model it was applied for numerical analysis of several semiconductor samples such as $ZnSe_{1-x}Te_x$ [8], $Zn_{1-x}Be_xSe$ [9], CdS_xSe_{1-x} [10] or $Cd_{1-x}Mn_xTe$ [11]. This method was also applied for other AII-BVI mixed crystals such as $Zn_{1-x}Be_xSe$ [12], $Zn_{1-x-y}Mg_yBe_xSe$ [13] or CdTe [14]. The constant question however was weather the applied model is correct for the situation observed for real semiconductor samples or not.

This paper is a comparison of the computations performed in a perfect uniform sample model and in a model of surface absorption.

2. Experimental Results

$Zn_{1-x}Be_xSe$ bulk crystals that were investigated were grown by the high pressure Bridgman method under argon overpressure in the range of composition $0<x<0.41$. The crystals were cut into 1–1.5mm thick plates and mechanically polished. The photoacoustic spectra were measured with the microphone phase sensitive method of detection.

The example experimental amplitude and phase photoacoustic spectra with the fittings of

 ISSN 1813-2065

theoretical curves for $Zn_{0.965}Be_{0.035}Se$ samples measured at f=25 Hz are presented in Fig. (1).

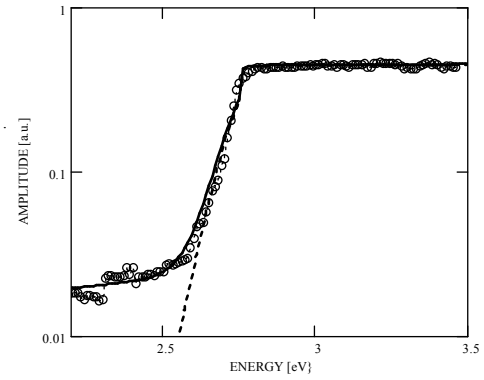

Fig. (1) Amplitude photoacoustic spectra of $Zn_{0.965}Be_{0.035}Se$ sample at f=25 Hz. Circles are experimental results, thick dashed lines are theoretical curves computed in the model of the volume absorption, thick solid lines are theoretical curves in the proposed model with the contribution of the surface absorption

In the volume absorption model the phase of the photoacoustic signal depends on the value of the optical absorption coefficient. For high values of the optical absorption coefficient the phase of the photoacoustic (PA) signal is equal to –90°. The low optical absorption value is accompanied by the phase shift of the photoacoustic signal going to –135° as it is shown by a dashed line in Fig. (2). In the surface absorption model, when light is absorbed only in a thin surface layer of a sample, the phase of the photoacoustic signal is independent on the value of the absorption coefficient and is always equal to –90°. Computations of the photoacoustic spectra in the surface absorption model were performed with two spatial temperature distributions given below

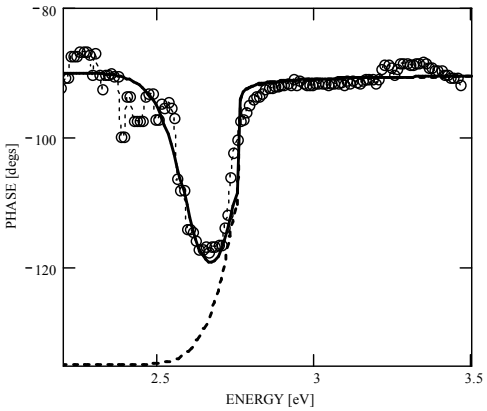

Fig. (2) Phase photoacoustic spectra of $Zn_{0.965}Be_{0.035}Se$ sample at f=25 Hz. Circles are experimental results, thick dashed lines are theoretical curves computed in the model of the volume absorption, thick solid lines are theoretical curves in the proposed model with the contribution of the surface absorption

a) for the volume absorption below the energy gap value:

$T_U(x, f, E, R, \beta_U(E), \alpha, l)$ (1)

Temperature distribution formula $T_U(x)$ was published elsewhere [15].

b) for the surface absorption below the energy gap value:

$$T_S(x,f,E,R,\beta_S(E),\alpha,l,d)=\frac{I_0\left[1-\exp(-\beta_S(E)d)\right]\cdot\left[\exp\left(-\sigma(f)x\right)+R\cdot\exp\left(-2\sigma(f)l+\sigma(f)x\right)\right]}{\lambda\sigma(f)\cdot\left[1-R\cdot\exp\left(-2\sigma(f)l\right)\right]} \quad (2)$$

where x is the spatial coordinate, f is the frequency of modulation , E is the energy of absorbed photons, R is the thermal reflection coefficient between the sample and the backing, $\beta_{U/S}(E)$ are the optical absorption coefficient formulae given by formula (5), d is the thickness of the surface layer, α is the thermal diffusivity, l is the thickness of the sample, $\gamma_{U/S}$ are thermal broadening coefficients, Eg is the energy gap value

The photoacoustic signal in a microphone detection in a front experimental configuration is given by formula (3).

$$PAS(f,E)=\frac{T_U(0,f,E,R,\beta_U(E),\alpha,l)\cdot\exp\left(-\beta_S(E)d\right)+T_S(0,f,E,R,\beta_S(E),\alpha,l,d)}{\sigma(f)} \quad (3)$$

Amplitude and phase of the PA signal are given by formulae (4).

$$AMP(PAS(f,E))=\left|PAS(f,E)\right|$$

$$PHASE(PAS(f,E))=\frac{180}{\pi}\arg\left(PAS(f,E)\right) \quad (4)$$

The PA amplitude and phase spectra computed in a volume absorption model are shown in figure 1a, b by dashed lines. This model however doesn't give satisfactory fittings for the low absorption region neither for the amplitude nor the phase photoacoustic spectra. Solid lines presented in Figs. (1) and (2) show theoretical curves computed in the model of the surface absorption. These curves exhibit much better fitting to experimental amplitude and phase photoacoustic spectra. Both theoretical spectra were computed for the same set of physical parameters presented below. The optical parameters obtained from the fitting of

theoretical curves (4) to experimental characteristics presented in Figs. (1) and (2) are given below:

Eg=2.75 eV	γ_U=0.50
l=0.1 cm	β_S=58 cm^{-1}
f=25 Hz	γ_S=0.01
β_U=80 cm^{-1}	α=0.03 cm^2/s

The optical absorption coefficient spectra of both the Urbach and surface absorption bands are of exponential type given by formula (5)

$$\beta_{U/S}(E) = \beta_{U/S} \cdot \exp\left[\frac{(E - Eg)\cdot\gamma_{U/S}}{0.025}\right] \qquad (5)$$

The photoacoustic spectra of the same sample but measured at f=15 Hz are presented in Figs. (3) and (4). Again it can be seen that the surface absorption model gives much better fitting of theoretical curves to experimental characteristics than the model of volume absorption.

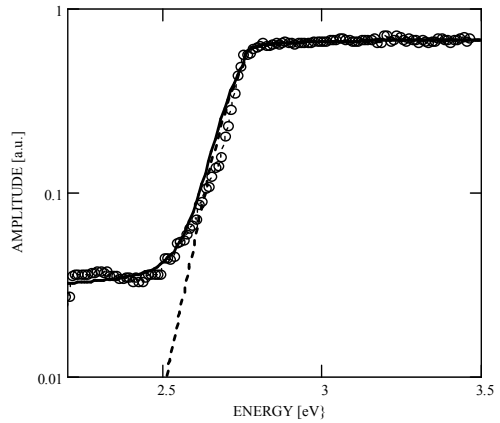

Fig. (3) Photoacoustic amplitude spectra of the $Zn_{0.965}Be_{0.035}Se$ sample but measured at f=15Hz. Circles are experimental values, dashed and solid lines are theoretical curves computed in the volume and surface absorption models, respectively

3. Conclusions

Computations and fittings presented in this paper show that for the proper determination of the optical absorption coefficient spectra of semiconductors the numerical analysis of both amplitude and phase spectra is necessary because the phase PA spectrum brings information about the type of absorption ie. volume or surface. As a consequence it results that it is not possible to compute the optical absorption coefficient spectrum in the region of low absorption only from the amplitude PA spectrum without the analysis of the phase spectrum. The surface absorption band is connected with the surface quality of the semiconductor samples and the measurement of the phase PA spectra can be a good test for its determination.

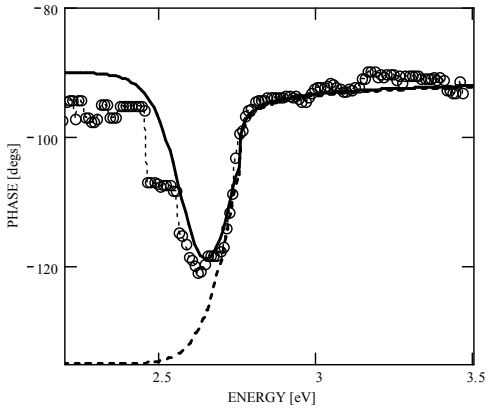

Fig. (4) Photoacoustic phase spectra of the $Zn_{0.965}Be_{0.035}Se$ sample but measured at f=15Hz. Circles are experimental values, dashed and solid lines are theoretical curves computed in the volume and surface absorption models, respectively

References

[1] A.C. Oliveira et al., *J. Magn. Magn. Mater.*, 252 56 (2002)

[2] P.C. Morais et al., *IEEE Trans. Magn.*, 39 2654 (2003)

[3] S. Decesari et al., *Atmosph. Chem. Phys.*, 6 375 (2006)

[4] P. Artaxo et al., *J. Geophys. Research*, Special Issue on LBA March 1 (2001)

[5] R. Cifelli et al., *J. Geophys. Research*, Special Issue on LBA December, 1 (2000)

[6] A. Rosenswaig and A. Gersho, *Science,* 190 556 (1975)

[7] P. Poulet, J. Chambron and R. Unterreiner, *J. Appl. Phys.*, 51, 1738 (1980)

[8] A.K. Gosh and B.K. Chaudhuri, *J. Appl. Phys.*, 80, 5292 (1996)

[9] B.K. Sarkar and B.K. Chaudhuri, *Int. J. Thermophysics*, 26 (1), 295 (2005)

[10] T. Toyoda and Q. Shen, *Anal. Sci.*, 17, s259 (2001)

[11] M. Nogaku and Y. Oka, *Jap. J. Appl. Phys.*, 30(11B), L1950 (1991)

[12] M. Maliński et al., in *Proc*. 6th Therminic Workshop Budapest (2000), p.93

[13] M. Maliński et al., *Anal. Sci.*, 17, (2001), s133

[14] L. Bychto and M. Maliński, in *Proc*. 28th Int. Conf. German Acoustic Society (2002), p.432.

[15] M. Maliński, *Archives of Acoustics*, 27(3), 217 (2002).

This article was reviewed at Department of Optics and Quantum Electronics, University of Szeged, Hungary, and School of Applied Sciences, University of Technology, Baghdad, Iraq

 ISSN 1813-2065

3rd International Conference on Digital Image Processing (ICDIP 2011)

April 15-17, 2011, China

3rd International Conference on Digital Image Processing (ICDIP 2011) is the premier forum for the presentation of new advances and research results in the fields of Digital Image Processing. The conference will bring together leading researchers, engineers and scientists in the domain of interest from around the world.

Topics of interest for submission include, but are not limited to:

Image acquisition
Image processing
Medical image processing
Pattern recognition and analysis
Visualization
Image coding and compression
Face Recognition
Super-resolution imaging
Image segmentation
Face recognition
3-D and Surface Reconstruction
Document analysis
Radar Image Processing
Sonar Image Processing
Signal Identification
Signal Reconstruction
Spectral Analysis
Filter Design
Adaptive Filters
Multi-channel Filtering
Noise Control
Fast Algorithms
Fast Fourier Transforms
Wavelet Transforms
Digital Signal Processing
Mobile Signal Processing
Statistical Signal Processing
Optical Signal Processing
Data Mining Techniques
Motion Detection
Content-based Image retrieval
Video Signal Processing
Watermarking
Detection and Estimation of Signal Parameters
Signal Identification
Nonlinear Signals and Systems
Time-Frequency Signal Analysis
Signal Reconstruction
Spectral Analysis
Filter Design and Structures
FIR Filters
IIR Filters
Adaptive Filters
Multi-channel Filtering
Signal Noise Control
Multiple Filtering and Filter Banks
Fast Algorithms
Adaptive and Clustering Algorithms
Fast Fourier Transforms
Discrete Cosine Transforms
Discrete Hilbert Transforms
Wavelet Transforms
Array Signal Processing
Digital Signal Processing
Statistical Signal Processing
Adaptive Signal Processing
Multidimensional Signal Processing
Mobile Signal Processing
Optical Signal Processing
Real Time Signal Processing
Higher Order Statistical Analysis
Cyclo-stationary Signal Analysis
Fuzzy Logic Applications in Signal Processing
Neural Networks for Signal Processing
Applications in Telecommunications
Industrial Applications

All accepted papers will be published in the conference proceeding by SPIE, which will be indexed by Ei Compendex and Thomson ISI.

Important Date

Paper Submission (Full Paper)	Before November 15, 2010
Notification of Acceptance	On December 15, 2010
Final Paper Submission	Before January 5, 2011
Authors' Registration	Before January 5, 2011
ICDIP 2011 Conference Dates	April 15 - 17, 2011

Tentative Submission Deadline : 15 November 2010

Homepage: http://www.icdip.org/cfp.htm

Investigations of Linear and Nonlinear Optical Properties of Transparent ZnO Thin Films Grown by Sol-Gel Method

Raad O. Al-Khayat
Osama M. Al-Taweel
Mahmood R. Al-Hadidi

Department of Physics, College of Education, University of Mosul, Mosul, Iraq

The optical properties of ZnO thin films grown by sol-gel method were studied using second and third harmonic generation and photoluminescence measurements, respectively. The structural properties of the ZnO thin films were carried out using x-ray method. The effects of the thickness variation and annealing temperature on the crystallinity parameters were observed.

Keywords: Zinc oxide, Thin films, Sol-Gel method, Nonlinear optics

1. Introduction

Zinc oxide (ZnO) is a wide-bandgap oxide semiconductor with a direct energy gap of about 3.37eV and a larger exciton binding energy (60 meV), which assures more efficient exciton emissions at higher temperatures. The ZnO thin films have attracted significant attention as a wide gap semiconductor due to their wide range of electrical and optical properties. They have potential application in electronics, optoelectronics and information technology devices including displays, solar cells and sensors [1,2].

Several thin-film deposition techniques have been used to produce pure ZnO films, including sputtering [3], molecular beam epitaxy [4], metal-organic chemical vapour deposition [5], pulsed laser deposition [6], spray pyrolysis [7] and the sol–gel process [8,9]. The sol–gel method has distinct potential advantages over these other techniques due to its ability to tune microstructure via sol–gel chemistry, a conformal deposition ability, compositional control and large surface area coating capability [10–12]. Undoped ZnO usually contains various

intrinsic defects such as Zn vacancies, interstitial Zn, O vacancies, interstitial O [13], and antisite O (O_{Zn}) [14]. These intrinsic defects form either acceptor level or donor level in the band gap that would greatly affect the optical properties of ZnO [14].

In the present work, we report optical linear and nonlinear properties of ZnO thin films prepared by sol-gel method. The main parameter of interest has been thicknesses of layers and pre-heating temperature.

2. Experiment

Zinc acetate 2-hydrate ($Zn(CH_3COO)_2.2H_2O$, 99.5%) was first dissolved at room temperature in a absolute ethanol as a solvent and diethanolamine ($HN(CH_2CH_2OH)_2$, DEA 99.0%) was added as a sol stabilizer. The concentration of zinc acetate was 0.75 mol/l and the molar ratio of DEA to zinc acetate was kept at 1.0. The solution was stirred at 70^{o}C for 30 min until it became clear and homogeneous to serve as the coating solution after aging for more than 24 h at room temperature. Silica glass and quartz wafers were used as substrate material after being cleaned in an ultrasonic bath for 15 min with acetone, ethanol and finally with distilled water. The wafers were then dipped into the solution and withdrawn at a rate of 6.0 cm/min. The coated substrate was dried at 60^{o}C for 10 min in air and then heated at a fixed temperature (120°C) for another 10min after each dipping procedure. To obtain a 200 nm thickness ZnO layers, this process was repeated four times. Next samples were annealing at various temperatures in the range of 250–550°C in air for 1 h.

In order to study the linear and nonlinear properties, a series samples were prepared with different number of layers (different thicknesses) and annealing at different temperature. X-ray diffraction (XRD) measurement of the ZnO films was carried out by an X-ray diffractometer utilizing CuK_α (λ=0.1542nm) radiation. Photoluminescence measurements were carried

 ISSN 1813-2065

out at room temperature excited by a HeCd laser at λ=325nm (E=3.815 eV)

3. Results and Discussion

Figure (1) shows the X-ray diffraction patterns of ZnO thin films deposited at room temperature and annealing in air at 450°C. Photoluminescence spectra of a ZnO thin film growing on fused quartz plates recorded at room temperature (RT) heating at different temperatures in the range of 250°C to 550°C are shown in Fig. (2).

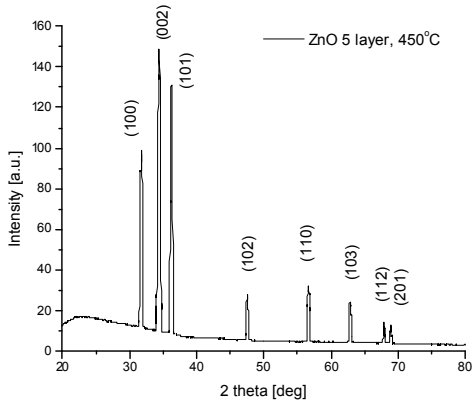

Fig. (1) XRD for 5 layer's ZnO thin film at heating temperature of 450°C

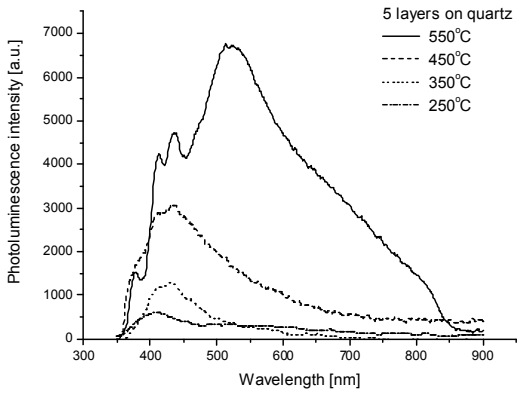

Fig. (2) Room temperature (298K) photoluminescence spectra of ZnO thin films deposited on fused quartz and annealing at different temperatures

The PL spectra for ZnO layers which were heated at different temperatures contained various emission features, which changed their intensity and positions with heating temperature. To determine the individual peak position and its intensity within a spectrum, we reconstructed the spectrum using multiple standard Gaussian equations. Near band edge (NBE) emissions at about 378nm are observed in the thin films heated at the temperatures higher than 250°C; however, for low annealing temperaturs we do not observed free exciton line. At 300K, the intensities of the excitons emission at 3.28eV (378 nm) and deep level (DL) peak at 2.30eV (540nm) are approximately equal.

The intensity of NBE emission increases with increasing annealing temperature. The DL emission with maximum near 2.30 eV (540 nm) is strong and very broad and is obsrved in all thin films. The DL emission includes the complete green, yellow and part of the red spectra. The relatively strong red emission peak is located near 1.68 eV (740 nm). This emission peak is associated with recombination centers in the crystal lattice of ZnO also originating through native defects [13,14]. For layer annealing at 550°C the emission line located at 3.37eV is attributed to free exciton, while the emission lines located at 3.32 and 3.23 eV are attributed to donor-acceptor pairs recombination.The increase of NBE emission compare to DL emission with annealing temperatures indicates that the high-optical quality thin film were obtained. Van et all. [13] found that the singly ionized oxygen vacancies are responsible for the blue and green emission in ZnO. From the above, it is possible that the emission at 2.30 eV (540nm) is connected with the oxygen vacancy introduced under annealing of ZnO layers.

Third order nonlinear optical susceptibilities ($\chi^{(3)}$) of ZnO thin films were examined by THG method. A Q-switched mode-locked Nd:yttrium–aluminum–garnet laser working at 1064nm with 16ps pulse duration, 1.62mJ power per pulse and 10Hz repetition rate was used.

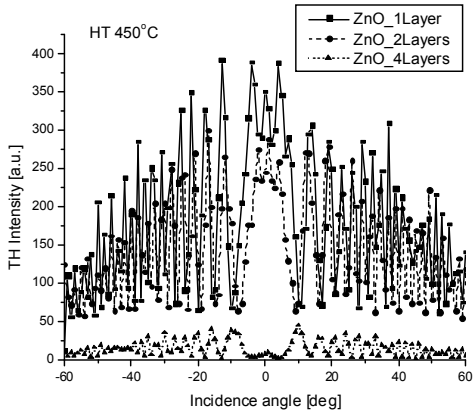

Fig. (3) THG signal versus incident angle of ZnO thin film for different number of layers

To determine the third order optical susceptibility of the sample, the analysis of the experimental results was carried out on the basis of the Maker fringes technique [13]. A typical result for THG measurement of ZnO thin films is shown in Fig. (3).

4. Conclusion

Good symmetry for THG singal was found and proved the smooth surface and good

crystallinity. The intensity of the signal decreases with increasing of thickness (number of layer) of thin film and also with increasing of heating temperature, except for RT. Table 1 shows the value of third order nonlinear optical susceptibilities ($\chi^{(3)}$) of ZnO thin films prepared with different method presented by other authors.

References

[1] S. Bandyopadhyay, G.K. Paul, S.K. Sen, Sol. Energy Mater. Sol. Cells 71 (2002) 103.
[2] Y. Natsume, H. Sakata, Thin Solid Films 372 (2000) 30.
[3] P. Nunes, D. Costa, E. Fortunato, R. Martins, Vacuum 64 (2002) 293.
[4] D.C. Look, D.C. Reynolds, C.W. Litton, R.L. Jones, D.B. Eason, G. Gantwell, Appl. Phys. Lett. 81 (10) (2002) 1830.
[5] K. Tominaga, T. Takao, A. Fukushima, T. Moriga, I. Nakabayashi,Vacuum 66 (2002) 505.
[6] N. Naghavi, C. Marcel, L. Dupont, A. Rougier, J.B. Leriche, C. Guery, J. Mater. Chem. 10 (2000) 2315.
[7] M. Krunks, E. Mellikov, Thin Solid Films 270 (1995) 33.
[8] T. Shuler, M.A. Aegerter, Thin Solid Films 351 (1999) 125.
[9] Y. Natsume, H. Sakata, Mater. Chem. Phys. 78 (2002) 170.
[10] E.J. Luna-Arredondo, A. Maldonado, R. Asomoza, D.R. Acosta, M.A. Melendez-Lira, M. de la L. Olvera, Thin Solid Films 490 (2005) 132.
[11] N.R.S. Farley, C.R. Staddon, L.X. Zhao, K.W. Edmunds, B.L. Gallagher, D.H. Gregory, J. Mater. Chem. 14 (2004) 1087.
[12] M. Ohyama, H. Kozuka, T. Yoko, Thin Solid Films 306 (1997) 78.
[13] K. Vanheusden, C.H. Seager, W.L. Warren, D.R. Tallant, J.A. Voigt, Appl. Phys. Lett. 68 (1996) 403.
[14] B. Lin, Z. Fu, Y. Jia, Appl. Phys. Lett. 79 (2001) 943.
[15 P.D. Maker, R.W. Terhune, M. Nisenoff , C.M. Savage, Phys. Rev. Lett. 8, (1962) 21.

This article was reviewed at Department of Physical Chemistry, University of Turku, Finland, and School of Applied Sciences, University of Technology, Baghdad, Iraq

---

 ISSN 1813-2065

International Conference on Sunrise Technologies (i-COST) 13-15 January 2011, India

International Conference on Sunrise Technologies (i-COST) is a flagship event of the SSVPS's B.S.DEORE College of engineering & polytechnic, DHULE. This conference tracks the successful organization of a national conference held in the previous year at our prestigious institutes. i-COST is a multidisciplinary event encompassing engineering areas related to the Computer, Civil, Mechanical, Electronics, information technology, automobile and Electronics & Communication. The broad multidisciplinary research areas of Engineering and Assistive Technologies contain some of the most challenging problems at the frontier of modern scientific research. They bring together researchers from many different disciplines with a shared, problem-centered approach, but seeking solutions utilizing technologies, skills and intellectual creativity from outside the traditional boundaries of engineering.

The objective of the conference is to provide an intellectual platform to professional engineers, academicians and research scholars of common interests to share novel concepts, experiences and knowledge in various fields of Engineering and Technology. The event provides an interactive dais of knowledge for Scientists, Engineers, Technocrats, Academicians, and Researchers. i-COST has a vital role to play in the process of streamlining and to decipher emerging theories and models in the technological field. i-COST has the onus to harness these with the common goal of uplifting our society and our globe at large and strive to prevent the fallout of possible ill effects in the era of mushrooming technologies.

The conference is structured in the format of plenary lectures followed by parallel sessions. The plenary lectures will be delivered by eminent personalities of international stature & repute to introduce the theme of the conference in their various domain expertise. Each parallel session will be addressed on specific topics followed by contributed papers. Such interactions will facilitate better understanding about technological developments across the world amongst the peers and academic fraternity. The conference will certainly ignite the minds of the researchers in undertaking research work to a greater elevation.

Papers are invited from the prospective authors from industries, academic institutions, and R&D organizations and from professional engineers. Potential topics to be addressed in this conference include, but are not limited to, the following,

The tracks for the conference are:

• Computer Science & Engineering
o Network & internet security
o Artificial intelligence & robotics
o Software Engineering
o Soft Computing
o Distributed Systems
o Parallel Computing
o Image Processing

• Civil Engineering
o Concrete and Structural Engineering
o Environment
o Infrastructure
o Building Science
o GIS

• Electronics Engineering
o Mechatronics (Interdisciplinary)
o Bio medical engineering
o Instrumentation Engineering
o Power Electronics & Systems
o Signal Processing & Communication Engineering.
o VLSI & Embedded Systems

• Mechanical Engineering
o Thermal engineering
o Production engineering
o CAD / CAM / CAE
o Automobile engineering
o Design Engineering

Prospective authors, intending to present their research papers, are requested to submit full length paper in the suggested format limited to double column 6-pages in MS Word. Maximum 3 authors can contribute for a paper. Papers should be submitted online through "easy chair" the link for the same is available on the website address http://ssvps.com/~icost/

Tentative Submission Deadline : 30 November 2010

Homepage: http://www.ssvps.com/~icost/

Optical Properties of Many-Layers Zinc Sulphide Thin Films prepared by Chemical Bath Deposition Method

Shakir M. Khalaf
Widad A. Hameed
Mohammed A.L. Al-Safi

Department of Chemistry,
College of Science,
University of Kufah,
Kufah, Al-Najaf, Iraq

Thin films of zinc sulphide have been prepared by chemical bath deposition in alkaline ammonia solutions from zinc acetate and thiourea, using successive depositions. The obtained films are amorphous. Air annealing did not improve the optical properties of the films with a too large number of layers.

***Keywords*:** Zinc sulphide, Thin films, CBD, Annealing

1. Introduction

In recent years, properties of nanosized materials have generated a great deal of interest because of the science involved in these studies and technological applications of these materials. As the physical dimensions of the particle approach to the nanometer scales, quantization and surface effects begin to play an important role, leading to drastic changes in the measured properties [1]. Semiconductor nanoparticles have attracted much attention because of their novel electric and optical properties originating from surface and quantum confinement effects [2-5]. ZnS is a II-VI semi conducting material with a wide direct band gap of 3.65eV in the bulk. It has potential applications in optoelectronic devices such as blue light emitting diodes [6], electroluminescence devices and photovoltaic cells which enable wide applications in the field of displays [7-8], sensors and lasers [9]. In recent years, nanocrystalline ZnS attracted much attention because the properties in nanoforms differ significantly from those of their bulk counterparts. Therefore, much effort has been made to control the size, morphology and polycrystallinity of the ZnS nanocrystals with a view to tune their physical properties. Hence, there has been growing interest in developing techniques for preparing semiconductor nanoparticles and films. The wet chemical synthesis method is a simple and inexpensive alternative to more complex chemical vapor deposition (CVD) and physical techniques. The physical methods [10], which are commonly used for the fabrication of nanomaterials, have some resolution limits that restrict these techniques from reaching the nanometer scale. On the other hand, the wet chemical technique offers a simple means to synthesize such particle with good control of size and size distribution [11].

Zinc sulphide is a binary II–VI semiconductor compound that is of interest in the technology of solar cells, photoconductive sensors and many others optical devices. Various techniques have been employed to prepare ZnS thin films, such as, metal-organic chemical vapour deposition [12], chemical bath deposition [13,14], SILAR method [15], electrodeposition etc. The chemical bath deposition (CBD) is an "electroless" technique that is attractive as low cost method. Unfortunately, the deposition parameters strongly influence the properties of the films: homogeneity, adherence to the support, crystalline structure, optical characteristics, etc.

The aim of this paper is to study the optical properties of some multilayer ZnS films prepared by CBD method. The transmittance (T) and the reflectance (R) of the films in the UV-Vis region, the value of the band gap energy (E_g) calculated from the transmittance spectra, and also the effect of the annealing process are reported.

2. Experiment

The ZnS films were prepared using a chemical bath containing zinc acetate (0.03 M), thiourea (0.60 M), sodium citrate (0.12 M) and ammoniac (0.30 M). Films were grown on optical glass slides in optimised conditions: temperature 84-86^0 C, pH 9.5-10.5. Thick samples were produced by successive deposition of 1 h layers. After each deposition, samples

 ISSN 1813-2065 Printed in IRAQ

were carefully washed and immersed into renew chemical bath. The optical glass slides of 30x45x1mm^3 used as support were cleaned using a special procedure.

Film thickness was determined by micro gravimetric weight difference method. The post–growth treatment of the samples consisted in 1 hour air annealing at 350^0, in an electrical furnace. Transmission spectra at normal incidence were recorded in the wavelength range of 300-900 nm using an UNICAM UV4 double beam spectrophotometer. Reflectance spectra at 8^0 angle e (specular reflectance included) and 0^0 (diffuse reflectance) incidence were obtained using the integrating sphere RSA-UC-40 accessory of the spectrometer.

3. Results and Discussion

Study of materials by means of optical absorption provides information on the quality of the thin films and some optical constants. A series of ZnS/glass/ZnS structures was prepared by a multi-step technique. The figure from sample notation indicates the number of the deposited layers by successively immersing the glass substrate into the chemical bath. The optical behaviour of samples was evaluated before and after the post-growth thermal treatment (samples noted adding TT). Optical measurements were performed on ZnS/glass/ZnS or ZnS/glass structures.

3.1 Zinc sulphide films characterization

XRD spectra showed that the as-grown zinc sulphide films possesses an amorphous structure Contrary to our expectation, the thermal post-growth treatment (1 h, 350°C in air) did not significantly changed the structural arrangement of film particles.

The optical transmittance of as-grown or annealed films, with different thickness is presented in Fig. (1).

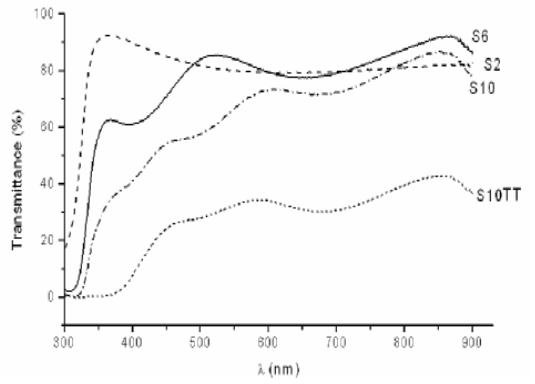

Fig. (1) Transmission spectra (corrected for glass absorption) of ZnS/glass/ZnS samples. The thickness of films is: 54 nm (S2), 208 nm (S6), 361 nm (S10) and 289 nm (S10TT)

As expected, the film transmission decreases as the thickness increases. In spite of the fact that during the annealing period the film thickness decreased, no improvement in the film transmittance could be observed. For instance, the thermal treatment reduces the transmittance of the sample S10 to about 30% (see Fig. 1). The pattern of interference fringes suggests that the films do not have uniform thickness.

The specular reflectance of samples calculated as difference of reflection measured at 8° (specular included) and 0° (diffuse reflectance) incidence decreased as the number of layers increased (Fig. 2). The consequence of the thermal treatment on the mirror type reflection of ZnS films was a slight improvement (sample S2) or an important reduction (sample S10). The evolution of optical characteristics of zinc sulphide films by the annealing process must be related to their multilayer structure that determined a grainy material and a possible contamination with zinc hydroxide.

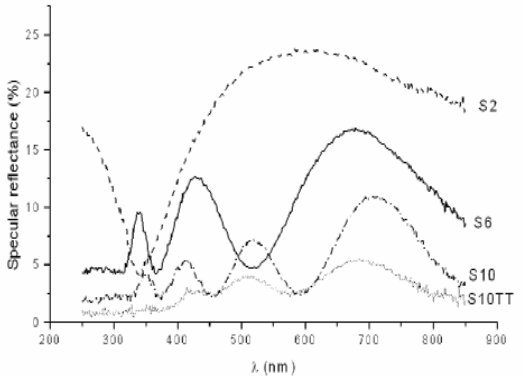

Fig. (2) Specular reflectance of ZnS/glass/ZnS samples

3.2 Optical constants of the films

Zinc sulphide is a direct band gap semiconductor, so that the absorption coefficient α can be related to the photon energy by:

$$(\alpha h\nu)^2 = A(h\nu - E_g) \qquad (1)$$

where A is a constant and E_g is the optical energy gap

From the transmittance spectra of ZnS/glass structures, the value of E_g was estimated by extrapolation of the straight line in the plot of $(\alpha h\nu)^2$ versus the photon energy $h\nu$ (Figure 3). The band gap of as-grown films is 3.6-3.75 eV, comparable to values reported by other authors for CBD prepared ZnS films [2].

The decreasing of band gap to 3.4–3.5 eV in the annealed films confirms the powdery nature, the non-uniformity of these films. The refractive index was calculated from the transmittance spectra according to Swanspoel's method, which assumes transparent and uniform films exhibiting interference patterns. The value of n (2.40-2.50)

systematic higher than data reported in literature for ZnS films (1.95-2.23, depending on deposition method [4]) or the bulk material (n~2.3) shows that the studied films are not enough uniform to give accurate values of maxim and minima of transmittance used in the calculus formula.

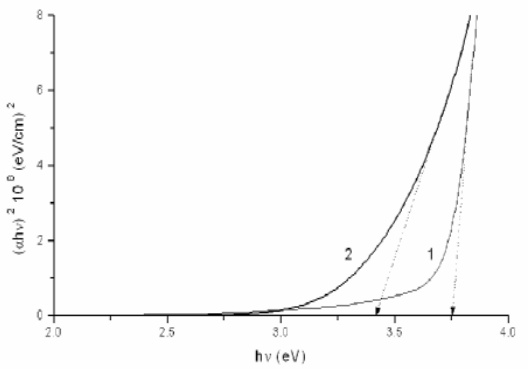

Fig. (3) Plot of $(\alpha h\nu)^2$ vs. $h\nu$ of sample S6 (ZnS/glass) as-grown (1) and annealed (2)

4. Conclusion

The investigation of the absorption and reflectance spectra of ZnS thin films grown on glass support, by CBD method using successive depositions, showed that the samples are amorphous and have a non-uniform thickness. The air thermal treatment at 350°C did not improve the optical properties of the films with a too large number of layers.

References

[1] A.P. Alivisatos, *Science*, 271 (1996) 933.
[2] G.Z. Wang et al., *Inorg. Chem. Commun.*, 4 (2001) 208.
[3] L.E. Brus, *Appl. Phys. A*, 53 (1991) 465.
[4] R. Maity and K.K. Chattopadhyay, *Nanotechnology*, 15 (2004) 812.
[5] S. Neeleshwar et al., *Phys. Rev. B*, 71 (2005) 201307(R).
[6] S. Coe et al., *Nature*, 420 (2002) 800.
[7] M.C. Beard, G.M. Turner, C.A. Schmuttenmaer, *Nano Lett.*, 2 (2002) 983.
[8] R.P. Raffaelle et al., *Prog. Photovoltaics*, 10 (2002) 433.
[9] V.I. Klimov et al., *Science,* 290 (2000) 314.
[10] A.P. Alivisatos, *Mater. Res. Soc. Bull.*, 23 (1998) 18.
[11] B. Zhang, J. Mu and D. Wang, *J. Dispersion Sci. & Technol.*, 26 (2005) 521.
[12] O. Osasona et al., *Optical Materials*, 7, 1997, 109-117.
[13] J.M. Dona and J. Herrero, *J. Electrochem. Soc.*,141, 1994, 205-210.
[14] I.C. Ndukwe, *Solar Energy Mater. Solar Cells*, 40, 1996, 123-131.
[15] S. Lindroos et al., *Materials Research Bulletin*, 33, 1998, 453-459.

This article was reviewed at School of Chemistry, University of Manchester, UK, and School of Applied Sciences, University of Technology, Baghdad, Iraq

 ISSN 1813-2065

The 2011 International Conference on Telecom Technology and Applications (ICTTA 2011)
13-14 May 2011 Australia

General Information
ICTTA is an annual International Conference on Telecom Technology and Applications sponsored by IACSIT and Singapore Institute of Electronics. ICTTA was started in Manila, Philippines (2009), held in Bali Island, Indonesia in 2010.
The 2011 International Conference on Telecom Technology and Applications (ICTTA 2011) will be held in Sydney, Australia during 13-14 May 2011. The aim objective of ICTTA 2011 is to provide a platform for researchers, engineers, academicians as well as industrial professionals from all over the world to present their research results and development activities in Telecom Technology and Applications. This conference provides opportunities for the delegates to exchange new ideas and application experiences face to face, to establish business or research relations and to find global partners for future collaboration.

Indexing
The ICTTA 2011 conference papers will be published in the proceedings, and will be included in the IEEE Xplore, and indexed by Ei Compendex and Thomson ISI and INSPEC.

Areas of Interest
Papers are invited on research in Telecom Technology and Applications, including but not limited to the following topics:

- Artificial Intelligence
- Algorithms and Techniques
- 3G & 4G Mobile Communication Services
- Agents and Multi-Agents systems for ICT Integrated Circuits for communications
- Antennas & Propagation
- Automation, Control and Robotics
- Bioinformatics and Bioengineering
- Biosignal Processing
- Business Information Systems
- Broadband & Intelligent networks
- Computational Intelligence
- Communication Systems
- Data Base Management
- Data Mining and Data fusion
- E-Commerce & E-government
- E-Health & Biomedical applications
- E-Learning & E-Business
- Emerging technologies & Applications
- Fuzzy, ANN & Expert Approaches
- Grid and Cluster Computing
- ICT & Banking
- ICT & Education
- ICT & Intelligent Transportation
- ICT in Environmental Sciences
- Image Analysis and Processing
- Image & Multimedia applications
- Information & data security
- Information indexing & retrieval
- Information Processing
- Information systems & Applications
- Internet applications & performances
- Knowledge Based Systems
- Knowledge Management
- Knowledge Management & Decision Making
- Machine Learning
- Machine Vision & Remote sensing
- Management Information Systems
- Mobile networks & services
- Network Management and services
- Networking theory & technologies
- Next generation network
- Optical Communications
- Pattern Recognition
- QoS management
- Satellite & Space Communications
- Signal & Image Processing
- Speech and Audio Processing
- Software Engineering and Formal Methods
- Systems & Software Engineering
- Web Engineering

Important Dates

Paper Submission (Full Paper)	Before January 5, 2011
Notification of Acceptance	On February 5, 2011
Authors' Registration	Before February 25, 2011
Final Paper Submission	Before February 25, 2011
ICTTA 2011 Conference Dates	May 13 - 14, 2011

Tentative Submission Deadline : 5 January 2011

Homepage: http://www.ictta.org/index.htm

THE IRAQI JOURNAL OF APPLIED PHYSICS
EDITORIAL BOARD

COPYRIGHT RELEASE
Iraqi Journal of Applied Physics (IJAP)

We, the undersigned, the author/authors of the article titled
……
……
……
……
……
……
that is presented to the Iraqi Journal of Applied Physics (IJAP) for publication, declare that we have neither taken part or full text from any published work by others, nor presented or published it elsewhere in any other journal. We also declare transferring copyrights and conduct of this article to the Iraqi Journal of Applied Physics (IJAP) after accepting it for publication.

The authors will keep the following rights:
1. Possession of the article such as patent rights.
2. Free of charge use of the article or part of it in any future work by the authors such as books and lecture notes without referring to the IJAP.
3. Republishing the article for any personal purposes of the authors after taking journal permission.

To be signed by all authors:

Signature:……..date: ……

Printed name: ……

Signature:……..date: ……

Printed name: ……

Signature:……..date: ……

Printed name: ……

Correspondence address:……...
……..
Address:……
……
……
Telephone:……..email: ……..

Note: Please complete and sign this form and mail it to the below address with your manuscript

The Iraqi Journal of Applied Physics
P. O. Box 55259, Baghdad 12001, IRAQ
Website: www.ijap.org
Email: editor@ijap.org
Phone: +964 7901274190

IRAQI JOURNAL OF APPLIED PHYSICS

CONTENTS

